


The coupled effect of tides and stellar winds on the evolution of compact binaries

Serena Repetto¹ and Gijs Nelemans^{1,2}

¹Department of Astrophysics/IMAPP, Radboud University Nijmegen, PO Box 9010, NL-6500 GL Nijmegen, the Netherlands

²Institute for Astronomy, KU Leuven, Celestijnenlaan 200D, B-3001 Leuven, Belgium

Accepted 2014 July 18. Received 2014 July 18; in original form 2014 May 1

ABSTRACT

We follow the evolution of compact binaries under the coupled effect of tides and stellar winds until the onset of Roche lobe overflow. These binaries contain a compact object (either a black hole, a neutron star or a planet) and a stellar component. We integrate the full set of tidal equations, which are based on Hut’s model for tidal evolution, and we couple them with the angular momentum loss in a stellar wind. Our aim is twofold. First, we wish to highlight some interesting evolutionary outcomes of the coupling. When tides are coupled with a non-massive stellar wind, one interesting outcome is that in certain types of binaries, the stellar spin tends to reach a quasi-equilibrium state, where the effects of tides and wind are counteracting each other. When tides are coupled with a massive wind, we parametrize the evolution in terms of the decoupling radius, at which the wind decouples from the star. Even for small decoupling radii, this *wind braking* can drive systems on the main sequence to Roche lobe overflow that otherwise would fail to do so. Our second aim is to inspect whether simple time-scale considerations are a good description of the evolution of the systems. We find that simple time-scale considerations, which rely on neglecting the coupling between tides and stellar winds, do not accurately represent the true evolution of compact binaries. The outcome of the coupled evolution of the rotational and orbital elements can strongly differ from simple time-scale considerations, as already pointed out by Barker and Ogilvie in the case of short-period planetary systems.

Key words: planets and satellites: gaseous planets – planet – star interactions – binaries: close – binaries: general – stars: magnetic field – stars: winds, outflows..

1 INTRODUCTION

Just like the Earth and the Moon, stars in binaries raise tidal bulges on each other. Tidal interaction is an important ingredient in binary evolution, and, on secular time-scales, it can drive the evolution of the system. Tidal interaction between two bodies dissipates energy, and induces exchange of angular momentum between the orbit and the spin of the components. See Zahn (2008) for a recent comprehensive review on tidal theory in binaries.

We study tidal interaction in binaries formed by a stellar component and a companion which can be approximated as a point mass, i.e. neutron star (NS), black hole (BH) or planet. Unless the spin angular momentum of the stellar component exceeds 1/3 of the orbital angular momentum, the binary orbital and rotational elements evolve in time, and the binary is pushed towards the lowest energy configuration, on a time-scale which depends on the strength of the tidal interaction. This configuration corresponds to a stable

solution for the evolution (Darwin 1879; Alexander 1973; Hut 1980). The equilibrium is characterized by circularity, tidal locking of the two components (synchronization) and alignment of the stellar spin with respect to the orbital spin. However, an equilibrium solution does not exist in case there is a sink of angular momentum in the system. A possible sink is any stellar wind which carries away angular momentum. One type of angular momentum loss we consider is *magnetic braking* (MB; see Parker 1958; Weber & Davis 1967; Verbunt & Zwaan 1981), the loss of angular momentum in a magnetic stellar wind from a low-mass star. The stellar wind, being anchored to the magnetic field lines, is forced to corotate out to large stellar radii, causing large amount of angular momentum being lost from the star and consequently from the orbit, thanks to the tidal coupling. Tides, counteracting the effect of MB, induce a secular spiral-in of the two stars, driving systems – that would otherwise remain detached – to Roche lobe overflow (RLO).

Tidal evolution is to be considered in all of those systems which acquire a certain degree of eccentricity and/or asynchronism at some point in their evolution. For instance, progenitors of black hole and neutron-star low-mass X-ray binaries (BH-LMXBs and

* E-mail: S.Repetto@astro.ru.nl

NS-LMXBs), systems containing a star and a planet, or binaries in globular clusters. Tides are also important in one of the possible models for long gamma-ray bursts, in which the black hole progenitor that undergoes core collapse is required to be a fast rotator. A way of enhancing the rotation of the progenitor is through synchronization with the orbital motion (see for example Church et al. 2012).

The coupling between tides and MB in the progenitors of black hole low-mass X-ray binaries (BH-LMXBs) and NS-LMXBs has often been neglected in the past; typically, one assumes that the binary rapidly circularizes and synchronizes. Once synchronization is achieved, every bit of angular momentum that is lost from the star is also lost from the orbit. We aim at investigating whether this model is a good description of the evolution of the systems. In order to do so, we numerically integrate the full set of tidal equations, coupled with MB, until the RLO configuration. We then compare our results with the estimates provided by the non-coupled method. We do the same for binaries containing a low-mass star with a planetary companion. We will extend our model to binaries where the stellar companion is of high mass, and we will see how the evolutionary equations need to be modified.

The effect of the coupling between tides and MB on the evolution of short-period extrasolar planetary systems was studied by Barker & Ogilvie (2009, hereafter BO2009). They found that neglecting MB in this type of systems results in a very different outcome of the evolution. And in particular, they concluded that it is essential to consider the coupled evolution of the rotational and orbital elements, a conclusion which was previously pointed out by Jackson, Greenberg & Barnes (2008), who also focused on the orbital evolution of planetary systems.

This paper is divided into six sections: in Section 2 we present our model and we validate our code, in Section 3 we show the binaries we study and we make some predictions of the evolution from simple time-scale considerations, in Sections 4 and 5 we show our results, and in Sections 6 and 7 we discuss our results and we draw our conclusions.

2 MODEL

2.1 Tides coupled with MB

MB is the loss of angular momentum in the stellar wind of a main-sequence (MS) magnetic star. Low-mass stars ($0.3 \lesssim M_* \lesssim 1.5 M_\odot$) have radiative cores and convective envelopes, where magnetic fields are thought to be amplified by dynamo processes. Thanks to the corotation of the magnetic field lines out to large distances from the star, any stellar wind takes away large amounts of angular momentum, even if the mass-loss is negligible. The braking is responsible for the slow rotation of most cool and old stars, like the Sun. From Skumanich's empirical law (Skumanich 1972) that describes the dependence of the equatorial velocity on age for MS G stars, the spin-down is obtained as

$$\frac{d\omega_*}{dt} = -\gamma_{\text{MB}} R_*^2 \omega_*^3, \quad (1)$$

where γ_{MB} is measured as $\approx 5 \times 10^{-29} \text{ s cm}^{-2}$, R_* is the radius of the star and ω_* is its spin frequency. For the radius of the star, we use the mass-radius relation of a zero-age main-sequence (ZAMS) star as in Tout et al. (1996). (Note that the star can grow by up to a factor of 2 on the MS). For a review on the different prescriptions of MB, see Knigge, Baraffe & Patterson (2011).

The star is doomed to lose its rotation within its MS lifetime, unless it is tidally coupled to a companion: the rotational angular momentum reservoir of the star is constantly being refuelled by the tidal torque.

We follow the Hut (1981) description of tidal interaction, in which tides have small deviations in magnitude and direction from their equilibrium shape, and where dynamical effects are neglected. In this model, the deviation of tides in magnitude and direction is parametrized in terms of a constant and small time lag τ . Orbital elements can therefore be assumed to vary slowly within an orbital period, and their change can be computed through averages along the orbit of the tidal potential.

We extend Hut's equations, valid in the small-angle approximation, to arbitrary inclinations of the stellar spin with the orbital spin, using the same orbit-averaged approach. We note that the tidal model by Hut (1981) was first extended to the case of arbitrary inclinations by Eggleton, Kiseleva & Hut (1998).

Taking a binary with semi-major axis a , spin frequency of the star ω_* , eccentricity e and inclination of the rotational angular momentum with respect to the orbital angular momentum i , we write the tidal equations for the evolution of the rotational and orbital elements, adding the MB term of equation (1):

$$\frac{da}{dt} = -6 \left(\frac{K}{T} \right)_i q(1+q) \left(\frac{R_*}{a} \right)^8 \frac{a}{(1-e^2)^{15/2}} \left[f_1(e^2) - (1-e^2)^{3/2} f_2(e^2) \frac{\omega_* \cos i}{\omega_{\text{orb}}} \right] \quad (2)$$

$$\frac{de}{dt} = -27 \left(\frac{K}{T} \right)_i q(1+q) \left(\frac{R_*}{a} \right)^8 \frac{e}{(1-e^2)^{13/2}} \left[f_3(e^2) - \frac{11}{8} (1-e^2)^{3/2} f_4(e^2) \frac{\omega_* \cos i}{\omega_{\text{orb}}} \right] \quad (3)$$

$$\frac{d\omega_*}{dt} = 3 \left(\frac{K}{T} \right)_i \frac{q^2}{k^2} \left(\frac{R_*}{a} \right)^6 \frac{\omega_{\text{orb}}}{(1-e^2)^6} \left[f_2(e^2) \cos i - \frac{1}{4} \frac{\omega_*}{\omega_{\text{orb}}} (1-e^2)^{3/2} (3 + \cos 2i) f_5(e^2) \right] - \gamma_{\text{MB}} R_*^2 \omega_*^3 \quad (4)$$

$$\frac{di}{dt} = -3 \left(\frac{K}{T} \right)_i \frac{q^2}{k^2} \left(\frac{R_*}{a} \right)^6 \frac{\sin i}{(1-e^2)^6} \frac{\omega_{\text{orb}}}{\omega_*} \left[f_2(e^2) - \frac{f_5(e^2)}{2} \times \left(\frac{\omega_* \cos i (1-e^2)^{3/2}}{\omega_{\text{orb}}} + \frac{R_*^2 a \omega_*^2 k^2 (1-e^2)}{M_{\text{comp}} G} \right) \right], \quad (5)$$

where M_{comp} is the mass of the compact companion, M_* is the mass of the star, q is the mass ratio M_{comp}/M_* , and the functions $f_i(e^2)$ are polynomials in e^2 as in Hut (1981). For the radius of gyration k , we use the fitting formula given in de Mink et al. (2013), which is based on the detailed stellar evolution models of Pols et al. (1998), and which gives the mass dependence of k .

The calibration factors $\{K/T\}_{i=c,r}$ measure the strength of the dissipation of the tidal flow. K is the apsidal motion constant, which takes into account the central condensation of the star (Lecar, Wheeler & McKee 1976). T is a typical time-scale on which significant changes in the orbit take place through tidal evolution; in units of the orbital period, T is the inverse of the tidal time lag τ . In his derivation, Hut considers a constant time lag τ . However, it has been later argued whether this was the appropriate choice. The time lag should in fact be compared with typical relaxation time of the process responsible for the dissipation. The source of

dissipation depends on the type of star which undergoes tidal deformations (see Zahn 1977).

Low-mass stars have convective envelopes, and it is believed that turbulent convection is responsible for the dissipation. When viscosity results from turbulence, the natural relaxation time is the eddy turnover time-scale τ_{conv} . This may be longer than the orbital period, in which case the efficiency of the dissipation should be reduced. The efficiency should then be dependent on the tidal forcing frequency (see Goldreich & Nicholson 1977; Zahn 1989; Ivanov & Papaloizou 2004).

Two scalings have been proposed for the viscosity due to the turbulent convection. Zahn (1966) assumes a linear scaling with the tidal forcing frequency. He expresses f_{conv} , the fraction of the convective cells which contribute to the damping, as

$$f_{\text{conv}} = \min \left[1, \left(\frac{P_{\text{tid}}}{2\tau_{\text{conv}}} \right) \right], \quad (6)$$

where P_{tid} is the tidal forcing period, given by

$$\frac{1}{P_{\text{tid}}} = \left| \frac{1}{P_{\text{orb}}} - \frac{1}{P_{\star}} \right|. \quad (7)$$

For high tidal forcing frequency (i.e. when $P_{\text{tid}} \ll \tau_{\text{conv}}$), the efficiency of momentum transfer by the largest convective cells is reduced. Instead, Goldreich & Nicholson (1977) suggested a quadratic dependence:

$$f_{\text{conv}} = \min \left[1, \left(\frac{P_{\text{tid}}}{2\tau_{\text{conv}}} \right)^2 \right]. \quad (8)$$

There is a longstanding uncertainty regarding which scaling is correct, with some numerical simulations of turbulent viscosity in a convection zone favouring a linear scaling (Penev et al. 2007), while others favouring a quadratic scaling (Ogilvie & Lesur 2012).

The question of tidal dissipation in a convective shell is still ‘Achille’s heel of tidal theory’, as Zahn (2008) wrote, and it goes beyond the scope of this paper. We choose f_{conv} as in equation (8). In this we follow the approach by Hurley, Tout & Pols (2002), Belczynski et al. (2008) and Valsecchi & Rasio (2014), who express the calibration factor for a convective envelope as

$$\left(\frac{K}{T} \right)_c = \frac{2}{21} \frac{f_{\text{conv}} M_{\text{env}}}{\tau_{\text{conv}} M_{\star}} [\text{yr}^{-1}], \quad (9)$$

where M_{env} is the mass in the convective envelope.

Zahn’s prescription seem to be in better in agreement with observations of tidal circularization times for binaries containing a giant star (Verbunt & Phinney 1995). A more recent work by Belczynski et al. (2008) showed the need for multiplying f_{conv} in equation (8) by 50, to match the observed circularization period of close binary stars. However, due to general uncertainties on tidal calibration for a convective envelope, we find our model a reasonable place to start.

Another uncertainty is whether and how the time lag should depend on the misalignment between the stellar spin and the orbital angular momentum. There is not yet agreement on this (Barker, private communication), and we prefer not to add additional parameters to our model.

High-mass stars have radiative envelopes, and tidal motions are assumed to be dissipated via radiative damping of the stellar g modes. In this case, the calibration factor is (Hurley et al. 2002; Belczynski et al. 2008)

$$\left(\frac{K}{T} \right)_r = 1.9782 \times 10^4 \frac{M_{\star} R_{\star}^2}{a^5} (1+q)^{5/6} E_2 [\text{yr}^{-1}], \quad (10)$$

where E_2 is a second-order parameter which measures the coupling between the tidal potential and the gravity mode (Zahn 1975); we fit it to the values given by Zahn (1975):

$$E_2 = 1.58313 \times 10^{-9} M_{\star}^{2.84} \quad (11)$$

(see also Hurley et al. 2002).

2.2 Non-coupled methods

One way of following the evolution of a binary system in which tidal friction and MB are both operating is to assume synchronization and to circularize the binary instantaneously or on a certain circularization time-scale, neglecting the spin of the star. The new semi-major axis is then $a_{\text{circ}} = a(1 - e^2)$. This choice appears reasonable when dealing with systems in which the angular momentum stored in the tidally deformed component is small (i.e. the moment of inertia of the star is small). Tidal interaction conserves the total angular momentum $J_{\text{tot}} = J_{\text{orb}} + J_{\star}$. Neglecting J_{\star} , conservation of J_{orb} gives $a_{\text{circ}} = a(1 - e^2)$. Afterwards, the tidal torque counteracts the effect of the magnetic spin-down, bringing angular momentum from the orbit back into the star. It is then reasonable to assume that every bit of angular momentum which is lost from the star is also lost from the orbit (i.e. $\dot{J}_{\text{orb}} = \dot{J}_{\star}$; see Verbunt & Zwaan 1981). The rate of angular momentum loss in the stellar wind is

$$\frac{dJ_{\star}}{dt} = k^2 M_2 R_{\star}^2 \frac{d\omega_{\star}}{dt}, \quad (12)$$

where we have neglected the change in radius and mass of the star, for the mass-loss being negligible (typically, $|\dot{M}_{\star}| \sim 10^{-14} M_{\odot} \text{yr}^{-1}$ for a Sun-like star). Using $\dot{a}/a = 2\dot{J}_{\text{orb}}/J_{\text{orb}} = 2\dot{J}_{\star}/J_{\text{orb}}$ and equation (1), and assuming $\omega_{\star} = \omega_{\text{orb}}$, the semi-major axis decay rate is

$$\frac{da}{dt} = - \frac{2\gamma_{\text{MB}} k^2 R_{\star}^4 G M^2}{M_{\text{comp}}} \frac{1}{a^4}, \quad (13)$$

where M is the total mass of the binary. We will call this approach *non-coupled* method.

Our approach instead is to numerically integrate the full set of tidal equations coupled with the magnetic spin-down (equations 2–5). In Section 4, we present the results of this integration for some illustrative binaries, showing how they differ from the results in the non-coupled method. A particular stress will be given to circularization time-scales. Some previous works used these time-scales as a simple way of depicting the evolution of compact binaries. It turns out that the true evolution of the eccentricity can highly differ from the exponential decay implied by the choice of a circularization time-scale as e/\dot{e} .

2.3 Validation of the evolution code

For small values of the inclination, our tidal equations for an eccentric and non-coplanar binary recover the equations in Hut (1981). In contrast to the BO2009 equations, we write down explicitly the tidal equations for $(a, e, \omega_{\star}, i)$ in the case of a non-circular and non-coplanar orbit. BO2009 choose instead of constant time lag τ like in Hut’s model a constant Q' , where Q' is a re-parametrization of the tidal calibration factor Q . The factor Q , also called *quality factor*, is a dimensionless quantity used mainly in planetary studies for characterizing the efficiency of tidal dissipation. BO2009 take $Q' = 10^6$ (see also Ogilvie & Lin 2007). We recover the equations 4–6 in BO2009 for a circular and non-coplanar orbit, when replacing K/T in our equations with $\frac{3}{2Q'} \frac{1}{\omega_{\text{orb}}} \frac{GM_{\star}}{R_{\star}^3}$.

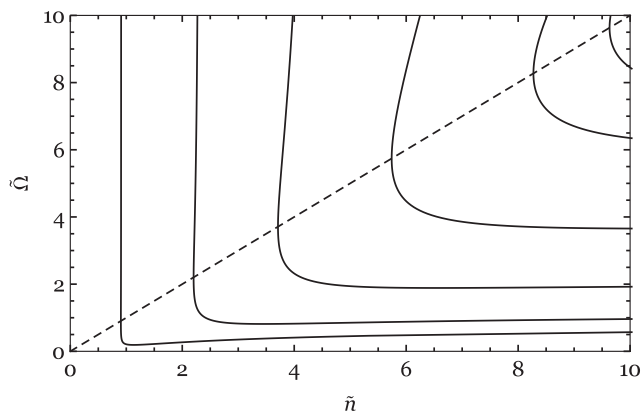


Figure 1. Evolution of a coplanar and circular planetary system with varying initial conditions in the plane $(\tilde{n}, \tilde{\Omega})$ (solid lines). The diagonal line corresponds to corotation $\tilde{\Omega} = \tilde{n}$.

In order to validate our code, we reproduce some of the results presented by BO2009. Fig. 1 is a phase-portrait plot, showing the evolution in the plane $(\tilde{n}, \tilde{\Omega})$ of coplanar and circular systems with varying initial conditions. The variables \tilde{n} and $\tilde{\Omega}$ are re-parametrization of the orbital frequency and the stellar spin frequency, respectively, which have been normalized to the orbital frequency at the stellar surface, together with a constant factor (see BO2009 for details). In integrating our evolutionary equations, we have replaced our tidal calibration factor K/T with $\frac{3}{2Q'} \frac{1}{\omega_{\text{orb}}} \frac{GM_*}{R_*^3}$, and we have used BO2009 calibration for magnetic braking (γ_{MB} in our model is 0.4 times smaller than γ_{MB} in BO2009). Fig. 1 coincides with the top plot in fig. 1 of BO2009. Once MB spins down the star below corotation ($\tilde{\Omega} < \tilde{n}$), the orbit undergoes tidally induced decay.

We also integrate our evolutionary equations for a set of planetary systems with circular and non-coplanar orbit ($i = 90^\circ$), and we show the corresponding solutions in the phase-portrait plot of Fig. 2. The overall evolution is similar to the one in Fig. 1, the only difference being that system with $\tilde{\Omega} \cos i < \tilde{n}$ undergoes orbital decay while still being outside corotation. This plot is identical to the top plot in fig. 3 in BO2009.

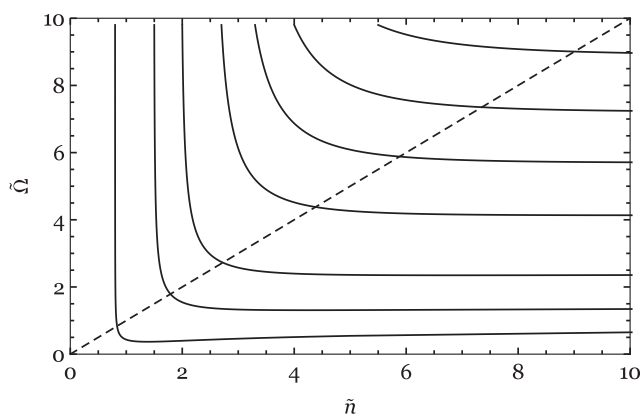


Figure 2. Evolution of a circular and non-coplanar ($i = 90^\circ$) planetary system with varying initial conditions in the plane $(\tilde{n}, \tilde{\Omega})$ (solid lines). The diagonal line corresponds to corotation $\tilde{\Omega} = \tilde{n}$.

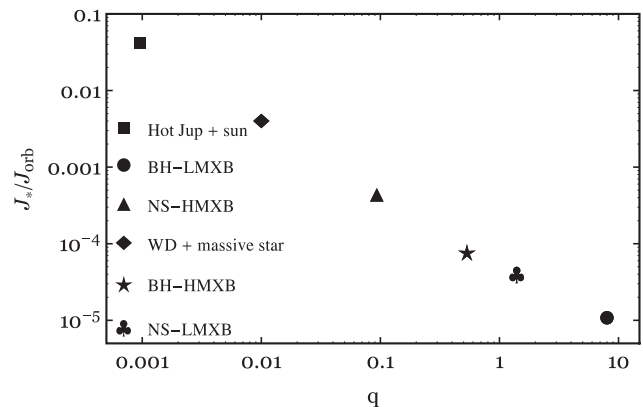


Figure 3. Different types of compact binaries as a function of the ratio J_*/J_{orb} between the rotational and the orbital angular momentum and as a function of the binary mass ratio q .

3 BINARIES IN OUR STUDY

We present the binaries we consider in our study in Fig. 3. The most extreme ones are binaries in which the magnetic wind from a low-mass star is coupled with the tidal friction between the star and its compact companion. The companion is either a black hole or a hot Jupiter, which is a planet with mass similar to Jupiter at a distance less than 0.1 au from its host star.

We will also extend our model to a case in which the star is of high mass instead (see Section 5). The companion is either an NS, a black hole or, in a more exotic scenario, a white dwarf (WD).

Together these systems span a wide range of mass ratios, ranging from $q = 0.001$ to 10.

We will refer to a binary containing a black hole or an NS as a black hole X-ray binary of high or low mass (BH-HMXB/BH-LMXB), or a neutron-star high/low-mass X-ray binary (NS-HMXB/NS-LMXB), where low and high refer to the mass of the companion. We point out though that these terms commonly refer to the mass-transfer phase, which is one of the evolutionary stages experienced by these binaries. What we deal with instead are systems on their way of becoming X-ray binaries, that is, we study the secular phase before mass transfer sets in.

3.1 Time-scale considerations

Before going into the details of the numerical integration of the coupled equations (2)–(3) and (4)–(5), we wish to make some predictions on the evolution of the systems based on simple time-scale considerations.¹

The binaries in our study are presented in Fig. 3 in terms of their mass ratio q and the ratio $\eta = J_*/J_{\text{orb}}$. J_{orb} is calculated for a circular orbit with $a = 2a_{\text{RLO}}$. a_{RLO} is the orbital separation at which the system undergoes RLO, i.e. $a_{\text{RLO}} = R_*/f(1/q)$, where $f(q)$ is a function of the mass ratio as in Eggleton (1983). J_* is calculated for a slow-spinning star with $\omega_* = 10^{-3} \omega_{\text{break}}$, where ω_{break} is the break-up frequency $\sqrt{GM_*/R_*^3}$. The ratio η is then larger for faster spinning star. It is an indicator for how much angular momentum is stored in the star compared to how much is stored in the orbit. A larger η , like in the planetary system case, implies

¹ As a note, throughout the paper we will indicate the time-scale of a certain event with τ , whereas t will indicate the time of occurrence of the same event in our integration.

that tides will more easily bring changes to the orbit than to the spin. If the orbit is sufficiently close, the planetary system suffers a significant tidal decay, while the tidal change of the stellar spin is much less significant. The opposite happens in a BH-LMXB, where tides easily affect the stellar spin.

The larger the mass ratio, the smaller the time-scale on which tides cause significant changes to the orbital and rotational elements, as can be seen from the dependence on the mass ratio of the tidal equations (2)–(5). Hence, tides are much more efficient in a BH-LMXB than in a planetary system.

We can obtain a rule of thumb for determining which systems will first circularize rather than synchronize. The circularization time-scale can be estimated as e/\dot{e} , where \dot{e} is as in equation (3), and assuming $e \approx 0$ and $\omega_* = \omega_{\text{orb}}$ (Hurley et al. 2002):

$$\frac{1}{\tau_{\text{circ}}} = \frac{21}{2} \left(\frac{K}{T} \right)_c q (1+q) \left(\frac{R_*}{a} \right)^8. \quad (14)$$

The synchronization time-scale for a circular orbit is calculated as (Hurley et al. 2002)

$$\frac{1}{\tau_{\text{sync}}} = \left| \frac{\dot{\omega}_{*|\text{tid}}}{\omega_* - \omega_{\text{orb}}} \right| = 3 \left(\frac{K}{T} \right) \frac{q^2}{k^2} \left(\frac{R_*}{a} \right)^6. \quad (15)$$

Then $\tau_{\text{circ}} < \tau_{\text{sync}}$ when

$$\frac{k R_*}{a} > \sqrt{\frac{6}{21} \frac{q}{1+q}}, \quad (16)$$

where the star can be modelled as a rigid sphere of radius kR_* . Taking $a = 2a_{\text{RLO}}$, the criterion is satisfied for two of the types of binaries we showed in Fig. 3: the planetary system and the binary consisting of a WD and a massive star. In all the other cases, we expect the first phase of the evolution of the binary to be driven by changes in the stellar spin rather than the orbit.

In our model, the spin is being affected both by tides and by MB; we compare their typical time-scales.

The MB spin-down time-scale is calculated as

$$\frac{1}{\tau_{\text{MB}}} = \frac{\dot{\omega}_{*|\text{MB}}}{\omega_*}, \quad (17)$$

where $\dot{\omega}_{*|\text{MB}}$ is as in equation (1). In Fig. 4, we show the synchronization time-scale and the circularization time-scale for a binary

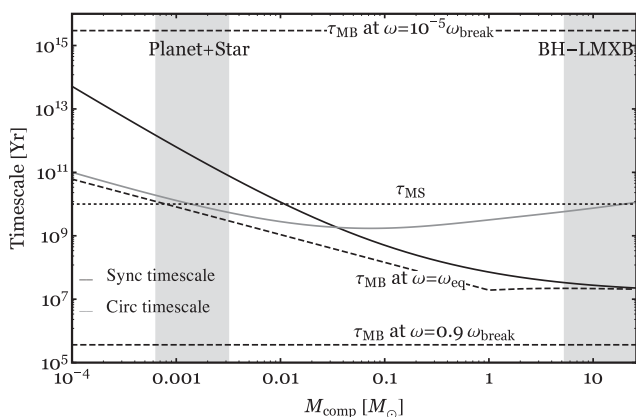


Figure 4. The solid black line and the solid grey line show, respectively, the synchronization and circularization time-scale for a binary with $a = 2a_{\text{RLO}}$ composed of a Sun-like star and a companion of mass M_{comp} . The dotted line shows the MS lifetime, whereas the dashed lines show the MB spin-down time-scale for $\omega_* = 0.9\omega_{\text{break}}$, the MB spin-down time-scale for $\omega_* = \omega_{\text{eq}}$ (see the text for details on ω_{eq}) and for $\omega_* = 10^{-5}\omega_{\text{break}}$.

composed of a low-mass star ($M_* = 1 M_{\odot}$), as a function of the compact companion mass (solid black and solid grey line). Time-scales are calculated using equations (14) and (15). The orbital separation is taken to be $a = 2a_{\text{RLO}}$ and the star is spinning with $\omega = 0.9\omega_{\text{break}}$. We also show the MS lifetime, the MB spin-down time-scale for a star spinning at $0.9\omega_{\text{break}}$, the MB spin-down time-scale for a star spinning at ω_{eq} and for a star spinning at $10^{-5}\omega_{\text{break}}$.

The quasi-equilibrium frequency ω_{eq} is the frequency at which MB and tidal torque are balancing each other (i.e. $|\dot{\omega}_{*|\text{MB}}| = |\dot{\omega}_{*|\text{tid}}|$, see Section 4 for further details). It has been calculated for an orbit with $a = 2a_{\text{RLO}}$ and $e = 0.1$.

For low mass ratios, tides are weak. Consequently, MB spins down the star below corotation ($\omega_* < \omega_{\text{orb}}$), and tides would not manage to synchronize the spin frequency to the orbital frequency within an MS lifetime. This is what happens in the planetary system case. Instead, in a BH-LMXB tides and MB tend to reach a quasi-equilibrium state in which they balance each other.

Concerning the circularization time-scale, it is typically shorter than the synchronization time-scale for $q < 0.05$, like in the planetary system case.

When tides and MB are coupled, we can use this figure to predict the evolution of the binary. If a star is initially spinning at $0.9\omega_{\text{break}}$, τ_{MB} is shorter than τ_{sync} . This means that in the first phase of the evolution MB spins down the star, until the time-scale on which tides act on the spin becomes comparable to the MB time-scale, and tides start playing a role.

4 RESULTS

4.1 Black-hole low-mass X-ray binary

The orbit of a BH-LMXB is typically eccentric right after the formation of the black hole. The eccentricity is the result of the mass ejection and/or possibly the natal kick in the supernova which gives birth to the black hole. In addition, any component of the natal kick perpendicular to the orbital plane will result in a misalignment between the orbital spin and the stellar spin. The most effective way of shrinking a BH-LMXB down to the RLO configuration is a coupling between the magnetic wind from the low-mass star and tidal friction, whereas gravitational wave emission can be neglected for the typical initial orbital separations ($a \approx 10R_{\odot}$).

Previous binary population synthesis (BPS) works on the evolution of BH-LMXBs have neglected the coupling between the stellar spin and the orbital spin, following the evolution of the binaries according to what we call the non-coupled method (see for example Kalogera 1999; Yungelson et al. 2006). This has been done for NS-LMXBs too; see for example Pylyser & Savonije (1988) and Ma & Li (2009). This choice was motivated by the fact that the rotational angular momentum is small compared to the orbital angular momentum. Also, the tidal evolution of the misalignment between the spin of the star and the orbital spin has usually been neglected.

4.1.1 An illustrative example of the evolution in the coplanar case

We integrate the tidal equations (2)–(5) for an illustrative system formed by a black hole of mass $M_{\text{BH}} = 8 M_{\odot}$ and a star of mass $M_* = 1 M_{\odot}$, until the RLO configuration is reached ($a_{\text{RLO}} \approx 4 R_{\odot}$). The rotational angular momentum is small compared to the orbital one (see Fig. 3); thus, we expect the system to rapidly reach the synchronous state.

In Fig. 5, we show the evolution for initial orbital parameters $a = 22 R_{\odot}$, $e = 0.7$ and $i = 0$. Concerning the spin of the star,

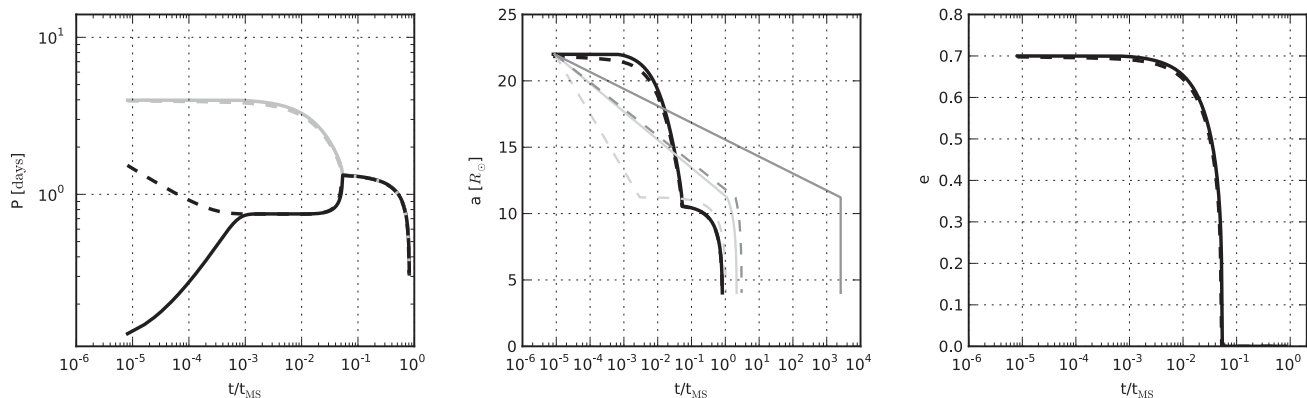


Figure 5. Evolution of a coplanar and eccentric BH-LMXB under the effect of tides and MB. The binary is composed of a black hole of mass $8 M_{\odot}$ and a $1 M_{\odot}$ star. Initial orbital parameters are $a = 22 R_{\odot}$, $e = 0.7$ and $i = 0$. We consider both a high-spinning star ($\omega_{\star} = 0.9 \omega_{\text{break}}$) and a low-spinning star ($\omega_{\star} = 10^{-5} \omega_{\text{break}}$). In all the three panels, the solid lines correspond to the high spin and the dashed lines to low spin. The left-hand panel shows the evolution of the stellar rotation period in black and of the orbital period in grey. The middle panel shows the evolution of the orbital separation, whereas the right one represents the evolution of the eccentricity. In the centre panel, the two thick black lines represent the evolution of the orbital separation in our integration. The thin dark grey lines represent the evolution of the orbital separation in the non-coupled method when taking $\tau_{\text{circ}} = (e/\dot{e})|_{e \approx 0, \omega_{\star} = \omega_{\text{orb}}}$ and thin light grey lines when taking $\tau_{\text{circ}} = e/\dot{e}$.

we consider both a star spinning at $\omega_{\star} = 0.9 \omega_{\text{break}}$ (see solid thick lines) and at $\omega_{\star} = 10^{-5} \omega_{\text{break}}$ (dashed thick lines).

Either via magnetic spin-down (high-spin case) or via tidal spin-up (low-spin case), the spin frequency converges to ω_{eq} , where ω_{eq} is the spin frequency such that $|\dot{\omega}_{\star, \text{MB}}| = |\dot{\omega}_{\star, \text{tid}}|$ (plateau in the left-hand panel in Fig. 5). The approach of this *quasi-equilibrium* state² is allowed by the fact that both $\dot{\omega}_{\star, \text{MB}}$ and $\dot{\omega}_{\star, \text{tid}}$ depend on the stellar spin (see equations 1 and 4).

Both solutions reach the quasi-equilibrium state ω_{eq} on a similar time-scale, which is very short ($\approx 10^{-3} t_{\text{MS}}$); therefore, no significant changes in the orbit take place during this phase. Afterwards, the orbit circularizes and the spin synchronizes to the orbital frequency. We note that the time for the orbit to become circular is non-negligible ($t_{\text{circ}} \sim 6 \times 10^{-2} t_{\text{MS}}$). Once synchronization and circularization are achieved, every bit of angular momentum which is lost from the star in the wind is also lost from the orbit. The two components effectively approach each other until RLO, and equation (13) describes well the evolution of the system. During this phase of the evolution, tides and MB are perfectly counteracting each other, i.e. $\dot{\omega}_{\star}|_{\text{MB}} = \dot{\omega}_{\star}|_{\text{tid}}$.

4.1.2 Comparison with non-coupled methods

We also compare the results of our integration with the estimates of the non-coupled method, both for the low-spin case and the high-spin case. The results are presented in the centre panel of Fig. 5, where we show the evolution of the semi-major axis in the non-coupled method. We take two types of circularization time-scale; one as in equation (14) (dark grey lines) and one given by $\tau_{\text{circ}} = e/\dot{e}$ (light grey lines). Solid lines are for the high-spin case and dashed lines for the low-spin case. The circularized orbital separation is overestimated in both scenarios, since changes in the orbit once the binary reaches the quasi-equilibrium state are neglected in non-coupled methods. As a consequence, the age of the binary at the RLO configuration is overestimated. When taking $\tau_{\text{circ}} = e/\dot{e}$, it is

overestimated by a factor of ≈ 2.6 in the high-spin case and by ≈ 1.3 in the low-spin case. The time it takes to reach circularization in our integration is $t_{\text{circ}} \approx 0.06 t_{\text{MS}}$. The ratio $t_{\text{circ}}/\tau_{\text{circ}}$ when taking $\tau_{\text{circ}} = e/\dot{e}$ is 0.05 in the high-spin case and 20 in the low-spin case. With τ_{circ} as in equation (14), the ratio is 2×10^{-5} and 0.03, respectively.

A better estimate of the time it takes to reach circularization would arise taking a star spinning at half the break frequency in the calculation of e/\dot{e} (see for details Fig. 7).

This illustrative example highlights the importance, at least in the first phase of the evolution (before circularization is achieved), of considering the coupled evolution of the rotational and orbital element.

4.1.3 An illustrative example of the evolution in the misaligned case

Misalignment has usually been neglected, and we wonder whether it brings significant changes to the orbital evolution. Due to the small angular momentum stored in the star ($J_{\star}/J_{\text{orb}} \ll 1$), we expect the tidal torque to easily affect J_{\star} . That is, we expect the stellar spin to rapidly align and synchronize with the orbital spin.

In Fig. 6, we show a representative illustration of the evolution of a BH-LMXB with initial orbital parameters $a = 9 R_{\odot}$, $e = 0.5$, with the star in a retrograde orbit around the black hole ($i = 120^{\circ}$) and spinning at $0.9 \omega_{\text{break}}$. Once MB has spun down the star sufficiently, the spin aligns with the orbital angular momentum. This can be seen in the right-hand panel in the figure, which shows how steeply the inclination decreases once the spin of the star has become negligible. An interesting difference with respect to the evolution in the coplanar case is the initial decay of the orbital separation in the retrograde orbit. This is due to the fact that $\omega_{\star} \cos i < \omega_{\text{orb}}$. In the retrograde case, or in any case when the previous condition is satisfied, there is a first phase in which tides and MB are simultaneously at work. In the coplanar case, instead, the first phase of the evolution is dominated either by tides or by MB, which act in opposite directions.

² We call it *quasi-equilibrium* state due to the fact that the orbital properties are still evolving.

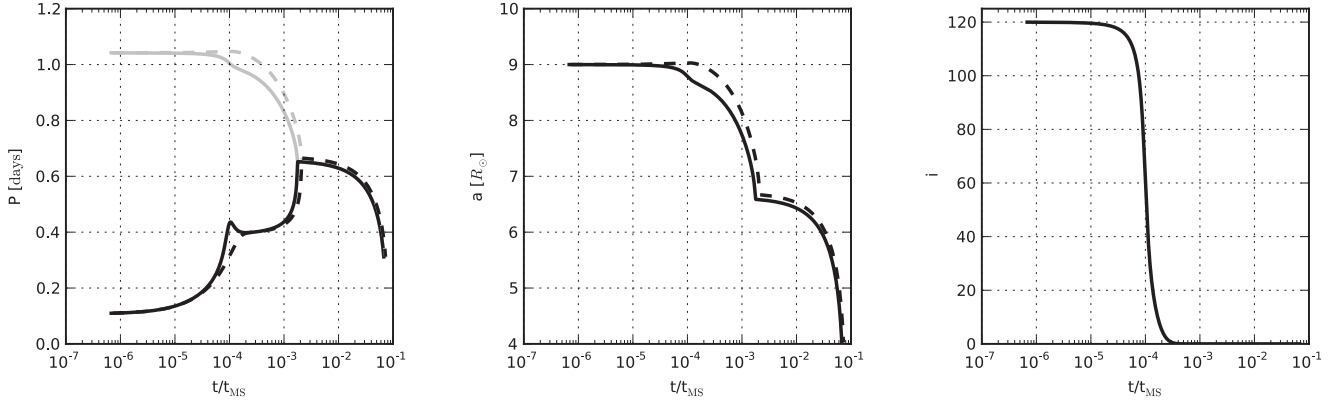


Figure 6. Evolution of a misaligned and eccentric BH-LMXB under the effect of tides and MB. The binary contains a black hole of mass $8 M_{\odot}$ and a $1 M_{\odot}$ star. Initial orbital parameters are $a = 9 R_{\odot}$, $e = 0.5$ and $i = 120^{\circ}$. The left-hand panel shows the evolution of the rotation period of the star (black solid line) and of the orbital period (grey solid line). The middle panel shows the evolution of the orbital separation (solid black line). The right-hand panel shows the evolution of the eccentricity (solid black line). The dashed lines in all of the three panels correspond to the evolution of a BH-LMXB with the same initial condition for (ω_*, a, e) , but with no misalignment between the spin and the orbit.

In case MB is not present, the star would align, but on a longer time-scale. This is due to the fact that MB is much more efficient than tides in spinning down the initially high-spinning star. Once the star has been spun down, the spin rapidly aligns. For the binary configuration, we have just showed the ratio between the time at which the spin aligns in the MB case and in the tides-only case is ≈ 0.6 .

4.1.4 Population study

As a more general diagnostic of the discrepancy between the coupled and the non-coupled method, we now do a population study, investigating how both the orbital separation at the time the binary circularizes and the time it takes to reach circularization change over the population. In the non-coupled method, the two quantities just mentioned are given by $a_{\text{circ}} = a(1 - e^2)$ and $\tau_{\text{circ}} = e/\dot{e}$.

The initial values e_0 of the eccentricity are taken from a grid which spans the interval $[0.001, 0.901]$. For each value of the eccentricity, we draw uniform values a_0 for the orbital separation in the interval $[a_{\text{min}}(e), a_{\text{max}}(e)]$. $a_{\text{min}}(e) = a_{\text{RLO}}/(1 - e)$ is the orbital separation at which the system undergoes RLO at periastron; $a_{\text{max}}(e)$ is the maximal orbital separation such that the system undergoes RLO within the MS lifetime. We draw uniform values $\omega_{*,0}$ for the stellar spin in the interval $[0, \omega_{\text{break}}]$ and uniform values i_0 in $[0^{\circ}, 180^{\circ}]$.

For each initial condition $(a_0, e_0, \omega_{*,0}, i_0)$, we integrate the tidal equations coupled with MB and we study the properties of 1000 solutions which undergo RLO within the MS lifetime. We calculate the ratio between the value in the coupled method and the value in the non-coupled method of the previously mentioned variables as a function of the eccentricity. We show the results in Figs 7 and 8.

For each value of the eccentricity, there is a range of values for $t_{\text{circ}}/\tau_{\text{circ}}$. The spread in the values at a fixed eccentricity is mainly caused by different initial spin frequencies. This was already seen in Fig. 5, where taking either a low-spinning star or a high-spinning star underestimates or overestimates t_{circ} .

To show how the spread in the ratio $t_{\text{circ}}/\tau_{\text{circ}}$ is reduced when fixing the initial spin of the star, we show in Fig. 7 the ratio $t_{\text{circ}}/\tau_{\text{circ}}$ when the initial spin is chosen to be $\omega_* = 1/2 \omega_{\text{break}}$ (dark grey shaded area). When we fix instead the orbital separation at birth [as

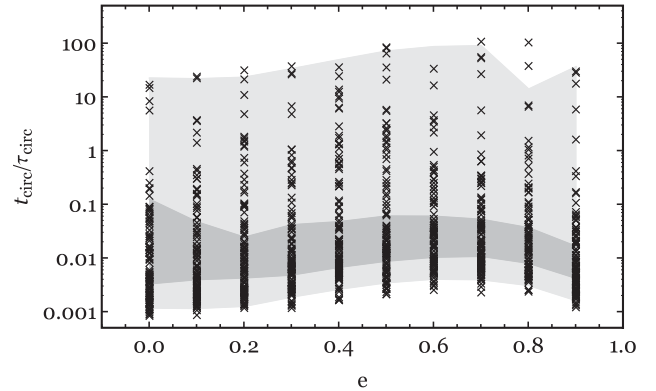


Figure 7. Ratio between the time it takes to reach circularization in the coupled and non-coupled method for 1000 BH-LMXBs undergoing RLO within the MS lifetime, when taking $\tau_{\text{circ}} = e/\dot{e}$. The light grey shaded area is for a fixed initial orbital separation and the darker grey area is for a fixed initial stellar spin.

an example, we take the average value between $a_{\text{min}}(e)$ and $a_{\text{max}}(e)$, the spread is conserved (light grey shaded area).

We also calculate the ratio $t_{\text{circ}}/\tau_{\text{circ}}$ when taking for τ_{circ} the expression in equation (14), see Fig. 9. The decrease in the ratio is caused by the dependence of τ_{circ} on the orbital separation, which increases with increasing eccentricities, and τ_{circ} increases accordingly.

Concerning the ratio between the orbital separation at $e = 0$ in our integration ($a_{e=0}$) and $a_{\text{circ}} = a(1 - e^2)$, it is typically less than 1. This is due to the fact that as soon as MB has spun down the star sufficiently, tides start removing angular momentum from the orbit, before synchronization is achieved. This effect is neglected in the non-coupled method. The decrease of the ratio with the eccentricity is a consequence of the a_{circ} dependence on $(1 - e^2)$.

We also calculate the ratio between the time it takes to reach the RLO configuration in our integration (t_{RLO}) and the estimated value for it in the non-coupled method (τ_{RLO}). In the non-coupled method, we calculate τ_{RLO} in two ways. One as $\tau_{\text{circ}} + t_{\text{VZ}}$, and the other as τ_{VZ} . In the first way, we integrate equation (13) taking as the initial condition $a_{\text{circ}} = a(1 - e^2)$; this gives t_{VZ} . We then calculate τ_{RLO} as

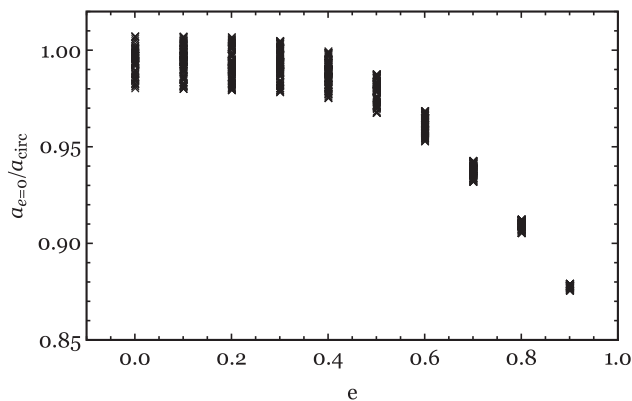


Figure 8. Ratio between the orbital separation at $e = 0$ and a_{circ} for 1000 BH-LMXBs undergoing RLO within the MS lifetime.

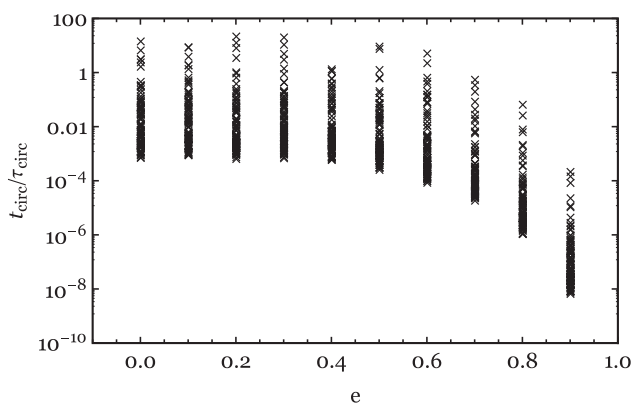


Figure 9. Ratio between the time it takes to reach circularization in the coupled and non-coupled method for 1000 BH-LMXBs undergoing RLO within the MS lifetime, when taking τ_{circ} as in equation (14).

$\tau_{\text{circ}} + t_{\text{VZ}}$, where $\tau_{\text{circ}} = e/\dot{e}$. The other way relies on assuming instantaneous circularization and taking $\tau_{\text{RLO}} = \tau_{\text{VZ}}$, where τ_{VZ} is a/\dot{a} with \dot{a} as in equation (13), and again we use $a_{\text{circ}} = a(1 - e^2)$ when calculating τ_{VZ} . This way of estimating τ_{RLO} has been mostly used in previous BPS works on the evolution of binaries hosting a black hole or an NS. We show the respective outcomes in Figs 10 and 11. The decrease in the ratio which appears in Fig. 11 is due to the fact that for higher eccentricities, both a_{min} and a_{max} increase; τ_{VZ} increases accordingly. When choosing τ_{RLO} as $\tau_{\text{circ}} + t_{\text{VZ}}$, the ratio is constrained to be in the interval (0.1–1), so we find this way of calculating τ_{RLO} a better estimate than when $\tau_{\text{RLO}} = \tau_{\text{VZ}}$.

4.2 Planetary system

We follow the evolution of a planetary system as well, composed of a Sun-like star and a hot Jupiter.

4.2.1 An illustrative example of the evolution in the coplanar case

We show an illustration of the evolution until the planet fills its Roche lobe (at $a_{\text{RLO}} \approx 2 R_{\odot}$) in Fig. 12. The initial configuration is $a = 4 R_{\odot}$, $e = 0.2$, $i = 0$, and we again consider the two cases of a high-spinning star ($0.9 \omega_{\text{break}}$) and a low-spinning star ($10^{-5} \omega_{\text{break}}$).

In the high-spin case, MB pushes ω_{\star} below corotation, and Hut’s stability condition is recovered within a short time-scale. Below

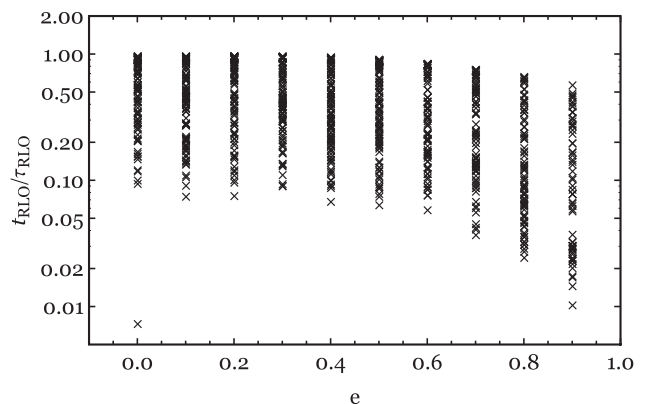


Figure 10. Ratio between the time it takes to reach RLO in the coupled and non-coupled method for 1000 BH-LMXBs undergoing RLO within the MS lifetime. In the non-coupled method, we take τ_{RLO} as $\tau_{\text{circ}} + t_{\text{VZ}}$ (see the text for details).

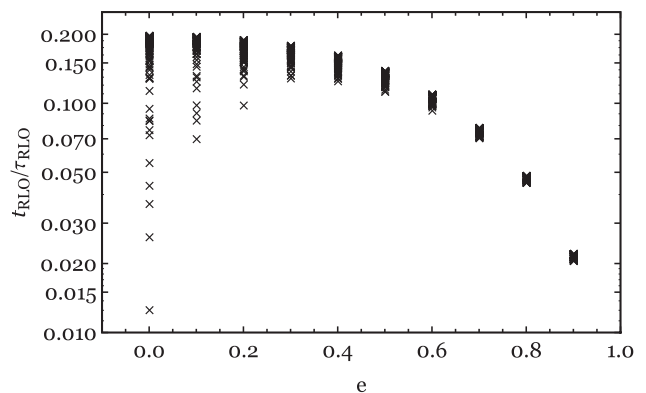


Figure 11. Ratio between the time it takes to reach RLO in the coupled and non-coupled method for 1000 BH-LMXBs undergoing RLO within the MS lifetime. In the non-coupled method, we take τ_{RLO} as τ_{VZ} (see the text for details).

corotation, tides are too inefficient for synchronizing the spin within the MS lifetime. The same result was found by BO2009 (see their fig. 3). The difference is that we use a different calibration factor causing tides in our model to be weaker. This is shown expressing the tidal calibration factor K/T as $\frac{3}{2Q'} \frac{1}{\omega_{\text{orb}}} \frac{GM_{\star}}{R_{\star}^3}$. This leads to $K/T \approx 7 \times 10^{-9}$ for the chosen initial conditions and $Q' = 10^6$, whereas in our model $K/T \approx 10^{-11}$, for every value of the initial spin. The weaker tides cause MB to spin down the star even more significantly below corotation.

In the BH-LMXB case, a condition in which $\dot{\omega}_{\star, \text{MB}} = \dot{\omega}_{\star, \text{tid}}$ is reached. This does not happen in the planetary case. The planetary system typically goes through one or two main evolutionary phases, each driven either by MB or by the tidal torque. In the high-spin case, the first phase is driven by MB until the spin finds itself below corotation, at which point the evolution is driven by the tidal interaction. In the low-spin case, the whole evolution is driven by tides. This overall behaviour of the solution persists in case the calibration factor is the one in BO2009. The stellar spin does not converge to the quasi-equilibrium characterized by $\omega_{\star} = \omega_{\text{eq}}$. In both tidal models, ω_{eq} is much smaller than typical ω_{eq} in BH-LMXBs (the corresponding $P_{\star, \text{eq}}$ is ≈ 21 d – see the dotted line in the left-hand panel of Fig. 12 – and ≈ 3 d in BO2009 model for

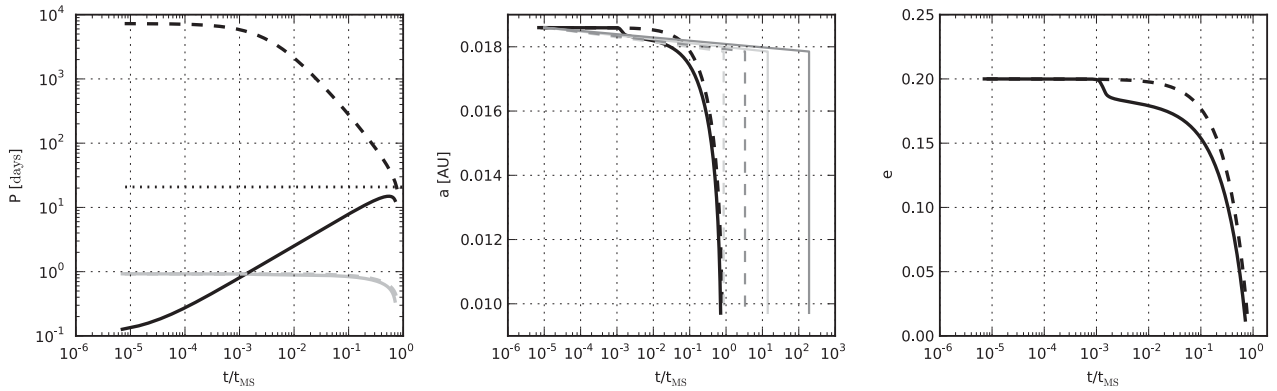


Figure 12. Evolution of an eccentric and coplanar planetary system under the effect of tides and MB. The system contains a hot Jupiter and a Sun-like star. Initial orbital parameters are $a = 4 R_{\odot}$, $e = 0.2$ and $i = 0$. We consider both a high-spinning star ($\omega_{\star} = 0.9 \omega_{\text{break}}$) and a low-spinning star ($\omega_{\star} = 10^{-5} \omega_{\text{break}}$). In all panels, solid lines correspond to high spin and dashed lines to low spin. In the left-hand panel, the grey lines represent the evolution of the orbital period and the black lines that of the stellar period. The dotted line in the same panel represents the value of ω_{eq} (see the text for details). In the centre panel, the two thick lines represent the evolution of the orbital separation in our integration. In the same panel, the thin dark grey lines represent the evolution of the orbital separation in the non-coupled method when taking $\tau_{\text{circ}} = (e/\dot{e})|_{e \approx 0, \omega_{\star} = \omega_{\text{orb}}}$ and light grey lines when taking $\tau_{\text{circ}} = e/\dot{e}$. The right-hand panel shows the evolution of the eccentricity.

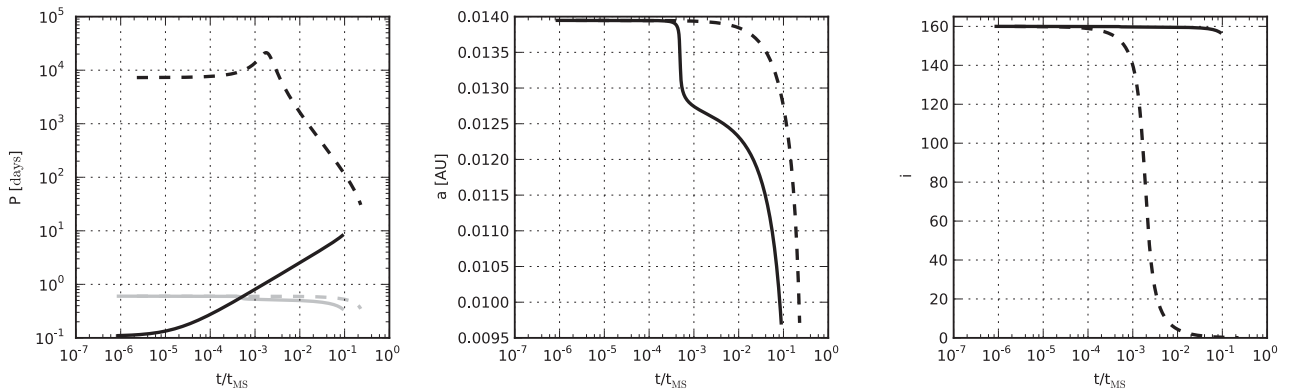


Figure 13. Evolution of an eccentric and misaligned planetary system under the effect of tides and MB. The system consists of a hot Jupiter and a Sun-like star. Initial orbital parameters are $a = 3 R_{\odot}$, $e = 0$ and $i = 160^{\circ}$. We consider both a high-spinning star ($\omega_{\star} = 0.9 \omega_{\text{break}}$) and a low-spinning star ($\omega_{\star} = 10^{-5} \omega_{\text{break}}$). In all panels, solid lines correspond to high spin and dashed lines to low spin. In the left-hand panel, the grey lines represent the evolution of the orbital period and the black lines that of the stellar period. In the centre panel, we show the evolution of the orbital separation. The right-hand panel shows the evolution of the misalignment angle.

tides). We will further comment on the absence or presence of the quasi-equilibrium state in Section 6.1. The only difference between the evolution in our model and that in BO2009 one is that in the low-spin case, the time it takes for tides to significantly spin up the star is shorter.

In the high-spin case, once ω_{\star} has been brought by MB below corotation (at $t \approx 10^{-3} t_{\text{MS}}$), tides start removing angular momentum from the orbit, the binary shrinks and the solution approaches the low-spinning solution, since the star now spins too slowly for MB to be effective.

In both cases of a high-spinning star and a low-spinning star, tides more easily bring changes to the orbit than to the star, due to the high ratio J_{\star}/J_{orb} (see Fig. 3), and in neither case the RLO configuration is synchronous, due to low mass ratio, unlike the BH-LMXB case.

In the middle panel of Fig. 12, we also show the evolution in the non-coupled method, when taking $\tau_{\text{circ}} = e/\dot{e}$ (thin light grey lines) and $\tau_{\text{circ}} = (e/\dot{e})|_{e \approx 0, \omega_{\star} = \omega_{\text{orb}}}$ (thin dark grey lines). Neglecting the

spin of the star results in a different evolution: the circularization time-scale is overestimated. At these large values of J_{\star}/J_{orb} , it is essential to follow the coupled evolution of the orbital and rotational elements.

4.2.2 An illustrative example of the evolution in the misaligned case

Due to the high ratio J_{\star}/J_{orb} , we expect tides to be inefficient in washing away any initial misalignment. In Fig. 13, we show the evolution of the planetary system for an initial configuration $a = 3 R_{\odot}$, $e = 0$, $i = 160^{\circ}$. The rate of alignment is larger in the low-spin case, whereas in the high-spin case, the star rotational angular momentum is too large for being affected by the tidal torque, and the system reaches RLO while being in a non-coplanar configuration. We might wonder what would happen to a retrograde orbit in the absence of

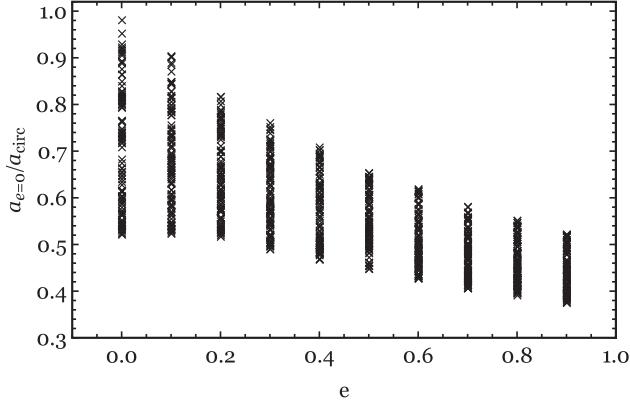


Figure 14. Ratio between the orbital separation at $e = 0$ and a_{circ} for 1000 planetary systems undergoing RLO within the MS lifetime.

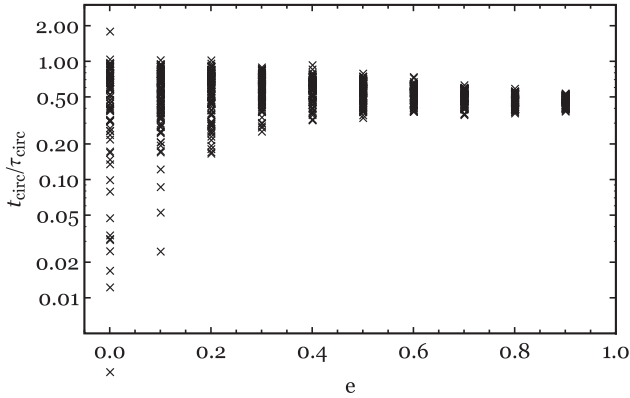


Figure 15. Ratio between the time it takes to reach circularization in the coupled and non-coupled method for 1000 planetary systems undergoing RLO within the MS lifetime.

MB. Taking the semi-major axis decay rate for a misaligned orbit (equation 2) and considering a circular case, the i -dependence of \dot{a} can be written as

$$\frac{da}{dt} \propto - \left(1 + \frac{\omega_* |\cos i|}{\omega_{\text{orb}}} \right). \quad (18)$$

The orbit would undergo an initial decay, with a larger rate for larger inclinations. This is an interesting way of shrinking the orbital separation, though the initial orbital separation has to be already comparable to a_{RLO} for RLO to happen on the MS. For example, for the case of an initial misalignment of 160° , the maximum initial orbital separation is $\approx 1.5 a_{\text{RLO}}$. The same orbital decay due to $\omega_* \cos i < \omega_{\text{orb}}$ happens in a BH-LMXB. In this case however, the system always reaches alignment and synchronization within the MS lifetime for sufficiently tight initial orbits, since the tidal torque is much larger.

4.2.3 Population study

We do a population study for the planetary system too, drawing the initial conditions in the same way as we did for the BH-LMXB case (see Figs 14 and 15). In the non-coupled method, τ_{circ} is again e/\dot{e} .

Again we see that a_{circ} typically overestimates the actual orbital separation at $e = 0$. Concerning the ratio of the time-scales, it spans a range of $\approx [10^{-2}-1]$. This is consistent with the example of Fig. 12.

5 WIND BRAKING

While most low-mass stars are magnetic, due to the dynamo processes undergoing in their convective envelopes, only a fraction of intermediate/high-mass stars show magnetic fields. This fraction is smaller than about 15 per cent of the total population, see Donati & Landstreet (2009). When the massive star is magnetic, the stellar wind becomes an analogue of the magnetic wind in a low-mass star, the only difference being that mass-loss is non-negligible anymore. We will take into account the effect of the mass-loss on the binary evolution adding a mass-loss term both in the orbital separation rate and in the spin-frequency rate. We will show that neglecting the spin-down rate due to the mass-loss leads to a different evolution.

5.1 Tides coupled with wind braking

Mass-loss in a stellar wind removes angular momentum from a rotating star. We assume that the wind is radial and isotropic; the wind can hence be modelled as a spherical shell decoupling from the star at a certain *decoupling radius* r_d . If the star is non-magnetic, r_d is the radius of the star R_* ; if it is magnetic, r_d is the magnetospheric radius r_M , i.e. the radius out to which the material corotates with the star.

Expressing the decoupling radius in terms of the stellar radius as $r_d = \gamma R_*$, the rate of angular momentum lost is then:

$$\frac{dJ_*}{dt} = \frac{2}{3} \dot{M}_* \omega_* \gamma^2 R_*^2 e_\omega, \quad (19)$$

where ω_* is the rotational frequency of the star. This expression coincides with the well-known prescription for the angular momentum loss in a stellar wind by Weber & Davis (1967), when parametrizing the Alfvén radius in terms of the stellar radius. It is valid both for a stellar wind decoupling at the stellar surface ($r_d = R_*$) and for a wind which is forced to corotate out to r_d by a purely radial magnetic field. For a different field geometry, this expression becomes

$$\frac{dJ_*}{dt} = \frac{2}{3} \dot{M}_* \omega_* R_*^2 \gamma^n e_\omega \quad (20)$$

recovering the purely radial field configuration for $n = 2$ (Kawaler 1988).

We assume that the wind decouples from the binary at r_d , without further interaction with the binary components. This is the so-called *fast-wind* approximation, motivated by the fact that typical wind speeds are larger than typical orbital speeds. In an NS-HMXB containing an NS of 1.4 and a $15 M_\odot$ star, $v_{\text{orb}} < 600 \text{ km s}^{-1}$ for $a > a_{\text{RLO}}$. Taking as wind velocity v_{wind} the escape velocity from the star, we obtain $v_{\text{wind}} \approx 1000 \text{ km s}^{-1}$.

To obtain the spin-down rate, we use the mass–radius relation for a ZAMS star, and we assume that the radius of gyration does not change during the evolution on the MS:

$$\frac{d\omega_*}{dt} = - \frac{\omega_*}{M_*} \dot{M}_* - \frac{2\omega_*}{R_*} \frac{dR_*}{dM_*} \dot{M}_* + \frac{2}{3} \frac{\dot{M}_* r_d^2 \omega_*}{k^2 M_* R_*^2}. \quad (21)$$

If the star is in a binary, the wind would not take away rotational angular momentum only, but orbital angular momentum as well. This effect adds up to the tidal effect on the orbital separation as a non-negative term $-\dot{M}_*/M$ in the orbital separation rate.

The full evolutionary equations for an eccentric and misaligned binary system under the coupled effect of tides and a massive stellar wind are equations (2)–(5), to which we add the term in equation (21) and the term

$$\frac{da}{dt} = - \frac{\dot{M}_*}{M} a \quad (22)$$

and we use the calibration factor $(K/T)_r$ for a radiative envelope.

The mass-loss for a Sun-like star on the MS is negligible; thus, we can neglect the term in equation (22). The mass-loss effect on the spin-down rate is reduced to the third term in equation (21). Even if the mass-loss is small, this term can be significant, when the decoupling radius is large ($r_d \approx 20 R_\odot$ for the Sun). The MB law (1) is empirical, and it can be recovered through magnetohydrodynamic theory coupled with theoretical studies of the dynamo process. Kawaler (1988) studied the angular momentum loss in low-mass stars and showed that Skumanich's law is recovered taking $n = 3/2$ in equation (20) and neglecting the change in mass and radius of the star.

The mass-loss in a fast isotropic wind always widens the orbit of a binary formed by point-like components, due to the decrease in binding energy. However, if the mass-losing star suffers from tidal deformation, the tides-induced torque can prevent the widening thanks to the redistribution of angular momentum. When $\omega_* < \omega_{\text{eq,tid}}$, where

$$\omega_{\text{eq,tid}} = f_2 (e^2) \omega_{\text{orb}} \left[\frac{1}{f_5 (e^2) (1 - e^2)^{3/2}} \right], \quad (23)$$

the tidal torque term in the spin rate is positive (see equation 4). This means that tides bring angular momentum from the orbit to the star, counteracting the effect of the mass-loss. We note that $\omega_{\text{eq,tid}}$ is alternatively referred to as *pseudo-synchronization* frequency, the synchronization frequency on an eccentric orbit (see Hut 1981). This is an *instantaneous*-equilibrium spin frequency, since orbital properties are still evolving. When the orbit is circular, this pseudo-synchronization frequency coincides with the orbital frequency.

In the next paragraph, we will estimate for which value of γ the effect of the tidal torque in decreasing the orbital separation is stronger than the effect of the orbital angular momentum loss in increasing it.

A few of the previous works on the evolution of high-mass X-ray binaries (HMXBs) have integrated the tidal equations coupled with the angular momentum loss in the wind (see for example Wong et al. 2012). What we do differently is to include in our set of equations the misalignment between the spin of the orbit and the stellar spin, and to parametrize the angular momentum loss in the wind in terms of γ , following the orbital evolution in a semi-analytical way and highlighting some interesting outcomes of the coupling between tides and a massive stellar wind.

5.2 Results

5.2.1 Timescale considerations

Let us assume that we have a synchronized, circular and coplanar orbit. The orbital separation changes due to the loss of orbital angular momentum (term of equation 22). It also changes due to the tidal redistribution of angular momentum. The star loses rotational angular momentum in the wind, and the tidal torque counteracts this effect. The effect of the tidal torque on the orbital separation can then be found from $\dot{J}_{\text{orb}} = \dot{J}_*$, which gives the orbital separation decay rate:

$$\left. \frac{da}{dt} \right|_{\text{tid}} = -\frac{4 |\dot{M}_*| \gamma^2 R_*^2 M}{3 M_{\text{comp}} M_* a}. \quad (24)$$

Taking the ratio between $\dot{a}|_{\text{ML}}$ and $\dot{a}|_{\text{tid}}$, we get

$$\frac{\dot{a}|_{\text{tid}}}{\dot{a}|_{\text{ML}}} = \frac{4}{3} \left(\frac{\gamma R_*}{a_2} \right)^2 q, \quad (25)$$

where a_2 is the distance of the star from the binary centre of mass, $a_2 = (M_{\text{comp}}/M)a$. The effect of the loss of J_{orb} is larger when the star is further away from the centre of mass (i.e. the larger a_2 is). Whereas, the effect of the tidal torque is larger, the larger the decoupling radius is (due to J_* -loss being larger), and/or the larger is the mass ratio (due to the tidal torque dependence on q).

We define γ_{min} as γ such that the condition $\left. \frac{da}{dt} \right|_{\text{tid}} = \left. \frac{da}{dt} \right|_{\text{ML}}$ is met. The tidal torque is more effective than the orbital angular momentum loss in changing the orbital separation for $\gamma > \gamma_{\text{min}}$:

$$\gamma_{\text{min}}(q, \eta) = \sqrt{\frac{3}{4q}} \frac{q}{1+q} \frac{\eta}{f(1/q)}, \quad (26)$$

where we parametrized the orbital separation in terms of the RLO separation, $a = \eta a_{\text{RLO}}$.

For an NS-HMXB composed of a $1.4 M_\odot$ NS and a $15 M_\odot$ companion,³ the mass ratio is $q \approx 0.09$, and taking $\eta = 2$, we find $\gamma_{\text{min}} \approx 0.83$. For the illustrative integration showed in Fig. 18, $\eta = 1.5$, and the corresponding γ_{min} is ≈ 0.6 . This means that *wind braking*⁴ wins over the mass-loss effect for every value of gamma. This remains valid when the companion mass spans a range of $[10-50] M_\odot$ in mass.

For a BH-HMXB composed of a $8 M_\odot$ BH and a $15 M_\odot$ companion, $q \approx 0.53$. We calculate $\gamma_{\text{min}}(q, 2) \approx 1.9$ and $\gamma_{\text{min}}(q, 1.5) \approx 1.6$. The latter γ_{min} corresponds to the initial conditions of Fig. 19. For smaller γ , we expect the orbital separation to grow in time (see the dotted line in Fig. 19). As another example we calculate the minimum gamma for the BH-HMXB Cygnus X-1. Its component masses are $M_* \approx 19 M_\odot$ and $M_{\text{comp}} \approx 15 M_\odot$ (Orosz et al. 2011). The correspondent γ_{min} for $\eta = 2$ is ≈ 2 .

In case WB is effective in shrinking the orbit, we wonder for which values of mass-loss in the wind and of γ , the binary is shrunk down to RLO within the MS lifetime. The spin-down time-scale due to the angular momentum loss in the wind is

$$\frac{1}{\tau_{\text{SD}}} = \frac{|\dot{\omega}_{*|\text{SD}}|}{\omega_*}, \quad (27)$$

where $\dot{\omega}_{*|\text{SD}}$ is as in equation (21). The spin-down time-scale is then a function of the mass-loss and of the decoupling radius. If the star is magnetic, we use the fact that the decoupling radius can be defined as the distance from the star at which the ram pressure of the flow and the magnetic pressure are balancing each other. Justham, Rappaport & Podsiadlowski (2006) show that

$$r_d \sim B_0^{1/2} R_*^{13/8} |\dot{M}_*|^{-1/4} (GM_*)^{-1/8}, \quad (28)$$

where B_0 is the surface stellar magnetic field. We use this expression for r_d in order to rewrite the spin-down time-scale (equation 27) in terms of B_0 and of \dot{M}_* . We are interested in those combinations of \dot{M}_* and B_0 for which the star is sufficiently spun down on the MS.

In Fig. 16, we show the ratio between the spin-down time-scale and the MS lifetime for a star of mass $15 M_\odot$ ($\tau_{\text{MS}} \approx 1.15 \times 10^7$ yr) as a function of the stellar surface magnetic field. Different curves are presented for different wind mass-losses. Mass-losses are chosen as $|\dot{M}_*| = \{10^{-9}, 10^{-8}, 10^{-7}, 10^{-6}\} M_\odot \text{ yr}^{-1}$. For larger

³ There are at least three known NS-HMXBs with similar component masses, see van Kerkwijk, van Paradijs & Zuiderwijk (1995), van der Meer et al. (2005) and Val Baker, Norton & Quaintrell (2005).

⁴ We name 'wind braking' (WB) the shrinking of the semi-major axis due to the tidal counteracting effect on the loss of rotational angular momentum, in analogy with magnetic braking.

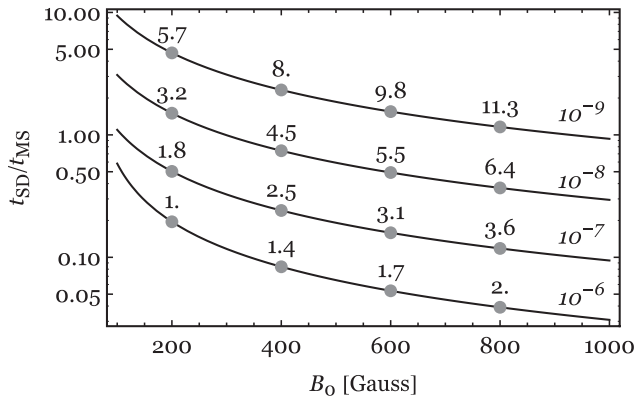


Figure 16. Ratio between the spin-down time-scale and the MS lifetime for a star of mass $15 M_{\odot}$, as a function of the stellar surface magnetic field for different mass-losses, $|\dot{M}_{\star}| = \{10^{-9}, 10^{-8}, 10^{-7}, 10^{-6}\} M_{\odot} \text{ yr}^{-1}$. Values of γ as a function of B_0 and \dot{M}_{\star} are indicated along the curves.

B_0 , the ratio decreases, since a stronger field guarantees the corotation of the field lines out to large distances from the star, where the rotational angular momentum carried away by the wind is larger. For the same magnetic field, the spin-down time-scale is smaller for larger mass-loss, since a higher mass-loss brings away a larger angular momentum. Along the curves we also indicate the value of $\gamma = r_d/R_{\star}$ for that combination of B_0 and \dot{M}_{\star} . For the same field strength at the surface B_0 , the decoupling radius is larger for a smaller mass-loss. This is due to the fact that for a smaller ram pressure (smaller \dot{M}_{\star}), the balancing magnetic pressure ($\sim B_0^2/r_d^6$) is smaller; if the surface B -field is fixed, the decoupling radius has therefore to be larger.

Typical magnetic fields of the subset of magnetic O-B stars and of Ap-Bp stars are of the order of hundreds to thousands gauss (Donati & Landstreet 2009). We compute their typical MS wind mass-loss using the fitting formula by Nieuwenhuijzen & de Jager (1990), who parametrize the wind mass-loss in terms of the luminosity, the mass and the radius of the star. Evolving a star with a ZAMS mass of $15 M_{\odot}$, with the single-star evolution (SSE) code by Hurley, Pols & Tout (2000) embedded in the Astrophysics Multipurpose Software Environment (Portegies Zwart et al. 2009), we extract the luminosity and radius of the star. We find a wind mass-loss in the range $10^{-8} - 10^{-7} M_{\odot} \text{ yr}^{-1}$ on the MS.

As an example, for a decoupling radius $\gamma = 2$ and a mass-loss $|\dot{M}_{\star}| = 10^{-7} M_{\odot} \text{ yr}^{-1}$, we obtain an estimate for the required stellar magnetic field of ~ 250 G. For these values of B and \dot{M}_{\star} , we expect the binary to shrink down to RLO.

In Fig. 17, we show the synchronization time-scales calculated using equation (15) for a binary formed by a star of mass $15 M_{\odot}$ as a function of the mass ratio q , both for an orbital separation $a = a_{\text{RLO}}$ and $a = 2 a_{\text{RLO}}$. The assumptions we make on the decoupling radius and the mass-loss rate are $\gamma = 2$ and $\dot{M}_{\star} = -10^{-7} M_{\odot} \text{ yr}^{-1}$ which, as can be seen in Fig. 16, allow for a short spin-down time-scale ($\tau_{\text{SD}}/\tau_{\text{MS}} \approx 0.3$). For our cases of interest of an NS-HMXB ($q \approx 0.1$) and of a BH-HMXB ($q \approx 0.5$), τ_{sync} is short; hence, we expect the binaries to rapidly reach the synchronous state.

5.2.2 WB in NS-HMXBs and BH-HMXBs

We integrate the coupled equations of Section 5.1 for a binary composed of an NS of mass $1.4 M_{\odot}$ and a $15 M_{\odot}$ star, with an orbital separation $a = 14 R_{\odot}$ and eccentricity $e = 0.2$.

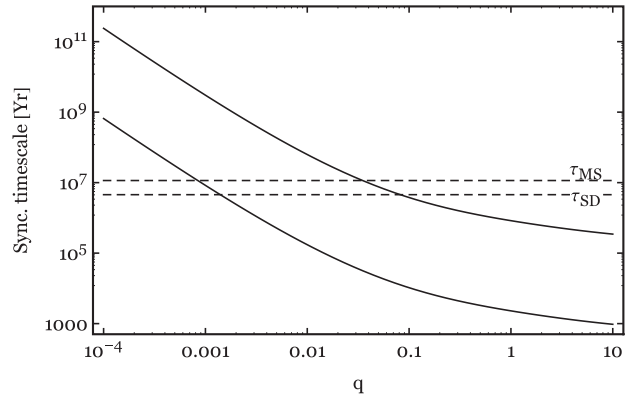


Figure 17. Synchronization time-scales for a binary composed of a $15 M_{\odot}$ star as a function of the binary mass ratio q , both for an orbital separation $a = a_{\text{RLO}}$ and $a = 2 a_{\text{RLO}}$. The horizontal dashed lines show the spin-down time-scale and the MS lifetime. The spin-down time-scale has been computed for $\gamma = 2$ and $\dot{M}_{\star} = -10^{-7} M_{\odot} \text{ yr}^{-1}$.

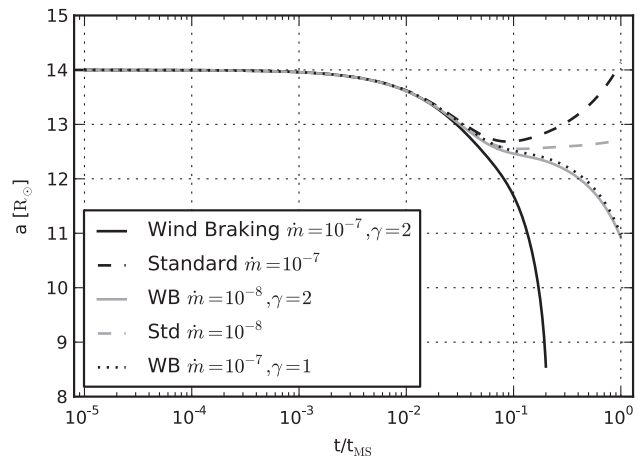


Figure 18. Evolution of an NS-HMXB under the effect of tides and a massive stellar wind (solid lines). Masses of the components are $M_{\star} = 15 M_{\odot}$ and $M_{\text{comp}} = 1.4 M_{\odot}$. Initial orbital parameters are $a = 14 R_{\odot}$, $e = 0.2$ and $\omega_{\star} = 0.2 \omega_{\text{break}}$. We also show the evolution in the standard scenario, when the mass-loss has an effect on the orbital separation only (dashed lines).

We take different combinations for the mass-loss rate and the decoupling radius: $\{|\dot{m}|, \gamma\} = \{\{10^{-7}, 2\}, \{10^{-8}, 2\}, \{10^{-7}, 1\}\}$ (where \dot{m} is the mass-loss rate in solar masses per year). For each of these three combinations, we also calculate the evolution when neglecting the mass-loss terms in the spin-frequency rate (terms in equation 21), which we call *standard* model. Concerning the spin frequency, we take a star rotating at 20 per cent of its break-up frequency, which is a typical lower limit on the natal rotating speed of a high-mass star (see Donati & Landstreet 2009). The associated ratio $\omega_{\star}/\omega_{\text{eq, tid}} \approx 0.7$. We must point out that this is valid in the assumption that the binary evolution prior and during the compact object formation does not affect the stellar spin. Anyhow, what is important for our study is to compare the initial ω_{\star} with $\omega_{\text{eq, tid}}$ of equation (23). Initial conditions with $\omega_{\star} > \omega_{\text{eq, tid}}$ are of no interest, since the binary widens, preventing RLO.

We show in Fig. 18 the outcome of the evolution. The first phase of the evolution is driven by tides, until synchronization is achieved

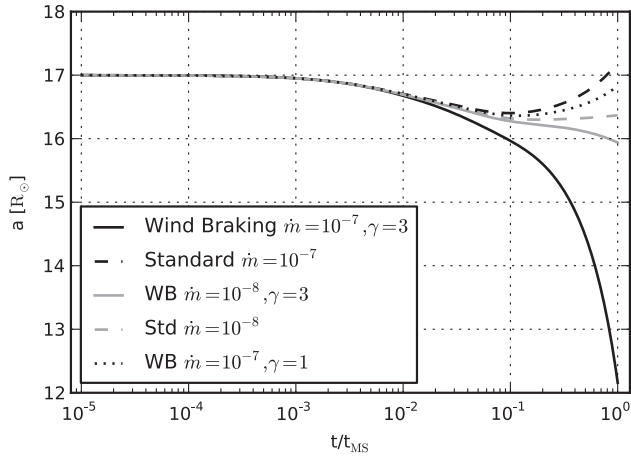


Figure 19. Evolution of a BH-HMXB under the effect of tides and a massive stellar wind (solid lines). Masses of the components are $M_* = 15 M_\odot$ and $M_{\text{comp}} = 8 M_\odot$. Initial orbital parameters are $a = 17 R_\odot$, $e = 0.2$ and $\omega_* = 0.2 \omega_{\text{break}}$. We also show the evolution in the standard scenario, when the mass-loss has an effect on the orbital separation only (dashed lines).

(at $t \approx 6 \times 10^{-2} t_{\text{MS}}$). At this moment, the different prescriptions on the decoupling radius and on the mass-loss rate start playing a role. When dealing with WB, the evolution is faster for a larger mass-loss. If the mass-loss is too small, the binary does not reach RLO within the MS lifetime. If the WB spin-down is not taken into account, the orbital separation increases once the synchronous state is achieved, as expected due to the positive wind mass-loss term in the orbital separation rate. For the WB solutions, once synchronization is achieved, the tidal torque replenishes the rotational angular momentum reservoir of the star, counteracting the spin-down effect of the wind and removing angular momentum from the orbit: this is exactly what happens in the MB case.

We also note how the two solutions with $\{|\dot{m}|, \gamma\} = \{10^{-7}, 1\}$ and $\{|\dot{m}|, \gamma\} = \{10^{-8}, 2\}$ only slightly differ from each other. This is due to the degeneracy in \dot{m} and γ . The spin-down time-scale is $\tau_{\text{SD}} \approx 2\tau_{\text{MS}}$ and $\tau_{\text{SD}} \approx 4\tau_{\text{MS}}$ for the two choices, respectively.

Solving the coupled equations for different values of the initial stellar spin, we note that if the initial spin is too low, tides would not manage to synchronize the star on the evolutionary time-scale. What happens is that the orbit keeps shrinking due to the tidal torque only, and there is no appreciable difference between the tides-only solution and the WB solution. The initial binary configuration (a , e , ω_*) which gives rise to an evolution of the WB type satisfies three properties. The stellar spin is less than $\omega_{\text{eq,tid}}$. The configuration allows for tides to synchronize the spin within the MS lifetime. Lastly, it allows the wind to significantly remove angular momentum from the orbit bringing the system to RLO within the MS lifetime.

We follow the evolution under tides and a massive stellar wind for a BH-HMXB as well. We take as initial orbital parameters $a = 17 R_\odot$, $e = 0.2$ and a star rotating at $0.2 \omega_{\text{break}}$. We show in Fig. 19 the result of the integration. We note how the solution with $\{|\dot{m}|, \gamma\} = \{10^{-7}, 1\}$ (dotted line) differs from the solution corresponding to the same pair $\{|\dot{m}|, \gamma\}$ for an NH-HMXB. This is due to the fact that $\gamma R_*/a_2$ is smaller for a BH-HMXB since a_2 is larger; this means that the tidal effect on the orbital separation is smaller. This was expected, since $\gamma = 1$ is less than the minimum value for having WB-type solutions in a BH-HMXB of this type.

6 DISCUSSION

In this section, we would like to comment on the calibration of MB and of tides that we chose. We also comment briefly on how our results on the evolution of a planetary system might change when considering the tides raised by the star on the planet as well.

(i) The empirical Skumanich law was derived measuring the equatorial velocity of G-type MS stars with rotational velocities between 1 and 30 km s⁻¹. It is therefore arguable whether it is still applicable to fast rotators, like the ones in compact binaries where the star, being synchronized with the orbit, rotates at velocities of hundreds km s⁻¹. For this reason, *saturated* MB laws have been suggested, in which the spin-down rate saturates once the star-frequency reaches a critical value (see Knigge et al. 2011, for reviewing the different MB prescriptions). We adopt the Ivanova & Taam (2003) prescription for MB in the formulation chosen by Ivanova & Kalogera (2006):

$$\dot{J}_{*,\text{MB}} = -K_j \left(\frac{R_*}{R_\odot} \right)^4 \begin{cases} (\omega_*/\omega_\odot)^3 & \text{for } \omega \leq \omega_x \\ \omega_*^{1.3} \omega_x^{1.7} / \omega_\odot^3 & \text{for } \omega > \omega_x, \end{cases} \quad (29)$$

where $\omega_\odot \approx 3 \times 10^{-6} \text{ s}^{-1}$ is the angular velocity of the Sun, $K_j = 6 \times 10^{30} \text{ dyn cm}$ and the critical angular velocity is $\omega_x = 10 \omega_\odot$. From this law, the spin-down rate $\dot{\omega}_*$ is derived.

We integrate the tidal equations coupled with the previous MB prescription for the BH-LMXB shown in Fig. 5, taking a star spinning at $0.9 \omega_{\text{break}}$, a value which is much larger than the critical angular frequency ω_x ; thus, the spin-down rate scales as $\omega_*^{1.3}$. In this prescription, MB is much less efficient than in the Verbunt & Zwaan (1981) prescription; hence, the binary does not reach RLO within the MS lifetime ($a \approx 5 a_{\text{RLO}}$ at $t = t_{\text{MS}}$). In the first phase of the evolution, MB spins down the star while tides lead to a slight widening of the orbit, unlike what happens in our formulation. In this case too, ω_* converges to ω_{eq} , which corresponds to the value at which $\dot{\omega}_{*,\text{MB}} = \dot{\omega}_{*,\text{tid}}$. After that, the binary shrinks thanks to the coupling between tides and MB, however much less significantly than when using the Verbunt & Zwaan (1981) prescription for MB.

(ii) There is a factor of $\approx 10^5$ difference between the time-scales in our model and those computed according to the BO2009 tidal model. This is due to the fact that K/T is a function of both ω_* and ω_{orb} , through the tidal pumping time-scale, whereas the calibration factor in BO2009 is a function of ω_{orb} only. When ω_* and ω_{orb} differ strongly (like in the case when $\omega_* = 0.9 \omega_{\text{break}}$), our tidal calibration factor is significantly reduced. Instead, when $\omega_* \approx \omega_{\text{orb}}$, the ratio between the two tidal calibration factors is 1–2 for every mass ratio, leading to similar time-scales.

(iii) We wonder whether our results are a function of the tidal calibration we choose. In the BH-LMXB case, a different tidal calibration factor will affect the time it takes for reaching the circular and synchronized configuration. However, since this time-scale is very short compared to the MS lifetime, independently of the chosen calibration, we expect no appreciable difference when taking a different tidal calibration factor. Once synchronization is achieved, the evolution of the system is well described by equation (13), that is, the calibration of tides does not play a role anymore. Integrating the tidal equations according to the BO2009 model for tides and coupling them with MB, we note that when the star is initially high-spinning, the orbital separation increases initially, that is in the first phase of the evolution tides and MB are both at work; this will lead to a larger circularized orbital separation, but the final outcome of the evolution of a BH-LMXB is not significantly affected. As a more quantitative test, we use the maximal initial orbital separation

a_{\max} such that the BH-LMXB reaches RLO within the MS lifetime; the ratio between a_{\max} in our model and that in the BO2009 model of tides is ≈ 1 , for all values of the initial eccentricity.

In the planetary system case, the situation is different. A high-spinning star is typically spun down below corotation. At this point, MB has a negligible effect, unlike the tidal interaction, and, if the initial configuration is close enough, tides bring the system towards RLO. The stronger the tides are, the faster the evolution towards RLO. Looking at the maximal initial orbital separation so that the planetary system reaches RLO within the MS lifetime, the ratio between a_{\max} in our model and that in the BO2009 model of tides is $\approx 0.3-0.4$.

(iv) When applying our model to the planetary case, we only considered the tide raised by the planet on the star, and not the tide raised by the star on the planet. Since the angular momentum stored in the planet is much less than the orbital angular momentum, due to the compactness of the planet, we expect the planet to rapidly synchronize with the orbit. If tides in the planet are included, we expect circularization to be reached faster, due to eccentricity damping effect of the tide in the planet (see BO2009 and Rasio et al. 1996). Matsumura, Peale & Rasio (2010) followed the evolution of a hot Jupiter in an eccentric and misaligned orbit around its host star, accounting for both the tide in the star and in the planet. The stellar tide largely dominates the evolution of the orbital separation and obliquity. Instead, both the tide in the planet and in the star contribute to the damping of the eccentricity, and depending on the planet tidal quality factor, circularization can be achieved without a significant orbital decay. We expect our main conclusions on the inadequacy of time-scale considerations to be preserved, as already predicted by Jackson et al. (2008), who accounted for the tide in the planet.

6.1 On the quasi-equilibrium state

The concept of *quasi-equilibrium state* for the spin of the stellar component in a binary was already introduced by Dobbs-Dixon, Lin & Mardling (2004), for the case of a planetary system containing a star and a hot Jupiter. At the quasi-equilibrium, the rate of angular momentum loss in the stellar wind is balanced by the rate at which the star gains angular momentum from the orbit as the planet attempts to spin up the star. The authors give an upper limit for the angular momentum loss in the stellar wind, such that this quasi-equilibrium can be achieved. We use a similar approach, and we calculate the maximum spin-down rate due to MB such that the quasi-equilibrium can be achieved. In order to find ω_{eq} , we put $\dot{\omega} = 0$ in equation (4), and we take a circular and coplanar orbit. We obtain

$$\omega_{\text{eq}} = \omega_{\text{orb}} - \frac{1}{3} \frac{1}{K/T} \frac{k^2}{q^2} \left(\frac{a}{R_*} \right)^6 |\dot{\omega}_{\text{MB}}|, \quad (30)$$

where a and ω_{orb} are the orbital separation and the orbital frequency at the quasi-equilibrium state. This quasi-equilibrium spin value is attainable provided that

$$|\dot{\omega}_{\text{MB}}| < \frac{9}{2Q'} \frac{q^2}{k^2} \frac{GM_* R_*^3}{a^6} = \dot{\omega}_{\text{max}}. \quad (31)$$

We note that we have chosen the calibration factor as in BO2009, that is we have replaced K/T with $\frac{3}{2Q'} \frac{1}{\omega_{\text{orb}}} \frac{GM_*}{R_*^2}$, so that the equation $\dot{\omega} = 0$ could be solvable analytically in terms of ω_{eq} . Condition (31) is typically not fulfilled in a planetary system, whereas it is fulfilled in a BH-LMXB (see Fig. 20). This is consistent with our results in Section 4.

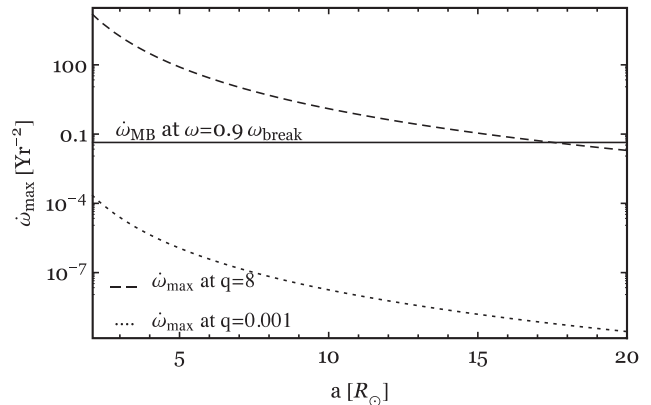


Figure 20. Values of $\dot{\omega}_{\text{max}}$ such that the system can reach the quasi-equilibrium state, as a function of the orbital separation, and calculated for a mass ratio $q = 8$ and for $q = 0.001$. Horizontal lines correspond to the spin-down rate due to MB.

6.2 An application to the NS-HMXB Circinus X-1

One way of testing the calibration of tides is to look at young and detached HMXBs, which still did not have time to circularize. In detached systems, any orbital decay or boost could be directly associated with the tidal interaction between the two components. Such a study was performed by Belczynski et al. (2008) for LMC X-4, an NS-HMXB. The observed orbital decay of the source, $P/\dot{P} \approx 10^6$ yr, is consistent with an orbital decay driven by the tidal torque when using the calibration factor in equation (10).

Another possible example is Circinus X-1, the youngest known X-ray binary. An upper limit on its age of $t < 4600$ yr has been placed by Heinz et al. (2013), through X-ray studies of its natal supernova remnant. The X-ray emission is thought to be caused by RLO at periastron; hence, this binary is semi-detached, unlike LMC X-4. X-ray dip timing shows that the binary is undergoing orbital decay (Parkinson et al. 2003; Clarkson, Charles & Onyett 2004), with P/\dot{P} measured to be ~ 3000 yr. The current orbital parameters are $e \approx 0.45$ and $P_{\text{orb}} \approx 16.68$ d. Jonker, Nelemans & Bassa (2007) constrained the radius of the companion star by ensuring that the NS does not go through the companion at periastron. The surface gravity gives in turn the mass. We use $M_* = 10 M_{\odot}$ and $R_* \approx 39 R_{\odot}$ for the mass and radius of the high-mass star, and $M_{\text{comp}} = 1.4 M_{\odot}$ for the mass of the NS. These initial conditions allow us to compute the current time-scales for the change in the orbital period $P/\dot{P} = (2/3)a/\dot{a}$, using the tidal equations in our model. The only uncertainty is the spin of the companion. When ω_* is smaller than $\omega_{\text{eq, tid}}$, tidal interaction results in a decay of the orbit. For these initial orbital parameters, $\omega_{\text{eq, tid}} \approx 1.25 \omega_{\text{break}}$. The calculated time-scales are $\approx 9 \times 10^3$ and $\approx 2 \times 10^4$ yr, for ω_* varying from 0 and $0.9 \omega_{\text{break}}$. One possibility is that tides are more efficient than the ones in our model, by a factor of ≈ 3 when taking a non-rotating star. Alternatively, the observed orbital decay is either induced by the mass transfer itself or an additional spin-orbit coupling is responsible for it, as suggested by Heinz et al. (2013).

6.3 Remarks on our results on the circularization time-scale and their consequences

(i) There are a variety of papers in the literature which base their description of the evolution of compact binaries on time-scale considerations (see, for example, Pylyser & Savonije 1988; Kalogera

1999; Yungelson et al. 2006; Ma & Li 2009). Since citing all of them does not seem like a sensible choice, we rather show an example of how time-scale considerations could fail. Janssen & van Kerkwijk (2005) study a compact binary formed by a pulsar and a low-mass star. The observed eccentricity is $e \lesssim 0.005$, while the initial eccentricity is constrained to be $e \sim 0.7$. The authors assume an exponential decay of the eccentricity when dealing with the circularization of the binary. We instead integrated our equations to solve for the evolution of the eccentricity of this system. We obtain $t_{\text{circ}} = 2 \times 10^9$ yr and $\tau_{\text{circ}} = 6 \times 10^7$ yr for a low-spinning star, and $t_{\text{circ}} = 4 \times 10^9$ yr and $\tau_{\text{circ}} = 2 \times 10^{10}$ yr for a high-spinning star. This result highlights the inadequacy of time-scale considerations when studying the evolution of individual systems.

(ii) We would also like to point out that some of the currently used BPS codes might treat tidal interaction using time-scale arguments or assuming instantaneous circularization (see, for example, Portegies Zwart & Verbunt 1996). However, our population models for the progenitors of BH-LMXBs show that the population of BH-LMXBs (i.e. the number of systems that start mass transfer on the MS) might not be very different, also given the large uncertainties in the calibration factor.

7 CONCLUSIONS

(i) The evolution of a binary formed by a point mass and a star can be solved relatively easily for arbitrary mass-loss, eccentricity and inclination via coupled differential equations. In this way, we can easily investigate how the evolution changes as a function of the binary mass ratio and of the ratio J_*/J_{orb} .

(ii) When tides are coupled with MB, the evolution of a BH-LMXB can be separated into two main phases. The first one is driven either by tides or by MB, depending on how fast the star is initially rotating. In both cases, the outcome of the first phase of the evolution is that the spin of the star converges to a quasi-equilibrium value at which $|\dot{\omega}_{*,\text{MB}}| = |\dot{\omega}_{*,\text{tid}}|$: the effect of the tidal torque and that of MB are balancing each other. From this moment on, every piece of angular momentum lost from the star is subtracted from the orbit.

(iii) In a planetary system instead, tides are too weak, and an initially high stellar spin is typically brought below corotation. From this point on, the evolution coincides with the evolution in the low-spin case. Unlike the BH-LMXB case, the binary does not reach the quasi-equilibrium state. If the star is initially high-spinning and highly inclined with respect to the orbital angular momentum, the RLO configuration is typically non-coplanar.

(iv) Models which neglect the coupling between tides and winds do not accurately represent the true evolution of compact binaries. The simple estimate τ_{circ} is not a good approximation for the actual change of e over time, because it does not account for the change in the orbital separation due to changes in the stellar spin. Nor for the fact that \dot{e} typically increases during the evolution, due to the decrease of the semi-major axis, whereas in the estimate e/\dot{e} the orbital separation a is assumed to be constant. Furthermore, neglecting the spin leads to an overestimate of the semi-major axis at circularization. It is then essential to consider the coupled evolution of rotational and orbital elements in order to accurately model the evolution of compact binaries. This was already showed previously by Jackson et al. (2008) and BO2009, for the planetary system case.

(v) We have implemented an easy model to follow the evolution of an HMXB under the coupled effect of tides and winds. For particular choices of decoupling radius and mass-loss, WB in a high-mass X-ray binary behaves as MB in a low-mass X-ray binary.

The values of decoupling radii and mass-losses which allow for a WB-type solution are consistent with typical magnetic fields and typical mass-losses of high-mass stars.

ACKNOWLEDGEMENTS

We thank the anonymous referee whose comments greatly improved the paper. SR is very grateful to Silvia Toonen for a careful and critical reading, which brought significant improvements to the manuscript. SR is also thankful to Adrian Barker for a useful discussion on the calibration of tidal dissipation. The work of SR was supported by the Netherlands Research School for Astronomy (NOVA).

REFERENCES

- Alexander M. E., 1973, *Ap&SS*, 23, 459
 Barker A. J., Ogilvie G. I., 2009, *MNRAS*, 395, 2268 (BO2009)
 Belczynski K., Kalogera V., Rasio F. A., Taam R. E., Zezas A., Bulik T., Maccarone T. J., Ivanova N., 2008, *ApJS*, 174, 223
 Church R. P., Kim C., Levan A. J., Davies M. B., 2012, *MNRAS*, 425, 470
 Clarkson W. I., Charles P. A., Onyett N., 2004, *MNRAS*, 348, 458
 Darwin G. H., 1879, *The Observatory*, 3, 79
 de Mink S. E., Langer N., Izzard R. G., Sana H., de Koter A., 2013, *ApJ*, 764, 166
 Dobbs-Dixon I., Lin D. N. C., Mardling R. A., 2004, *ApJ*, 610, 464
 Donati J.-F., Landstreet J. D., 2009, *ARA&A*, 47, 333
 Eggleton P. P., 1983, *ApJ*, 268, 368
 Eggleton P. P., Kiseleva L. G., Hut P., 1998, *ApJ*, 499, 853
 Goldreich P., Nicholson P. D., 1977, *Icarus*, 30, 301
 Heinz S. et al., 2013, *ApJ*, 779, 171
 Hurley J. R., Pols O. R., Tout C. A., 2000, *MNRAS*, 315, 543
 Hurley J. R., Tout C. A., Pols O. R., 2002, *MNRAS*, 329, 897
 Hut P., 1980, *A&A*, 92, 167
 Hut P., 1981, *A&A*, 99, 126
 Ivanov P. B., Papaloizou J. C. B., 2004, *MNRAS*, 353, 1161
 Ivanova N., Kalogera V., 2006, *ApJ*, 636, 985
 Ivanova N., Taam R. E., 2003, *ApJ*, 599, 516
 Jackson B., Greenberg R., Barnes R., 2008, *ApJ*, 678, 1396
 Janssen T., van Kerkwijk M. H., 2005, *A&A*, 439, 433
 Jonker P. G., Nelemans G., Bassa C. G., 2007, *MNRAS*, 374, 999
 Justham S., Rappaport S., Podsiadlowski P., 2006, *MNRAS*, 366, 1415
 Kalogera V., 1999, *ApJ*, 521, 723
 Kawaler S. D., 1988, *ApJ*, 333, 236
 Knigge C., Baraffe I., Patterson J., 2011, *ApJS*, 194, 28
 Lecar M., Wheeler J. C., McKee C. F., 1976, *ApJ*, 205, 556
 Ma B., Li X.-D., 2009, *ApJ*, 691, 1611
 Matsumura S., Peale S. J., Rasio F. A., 2010, *ApJ*, 725, 1995
 Nieuwenhuijzen H., de Jager C., 1990, *A&A*, 231, 134
 Ogilvie G. I., Lesur G., 2012, *MNRAS*, 422, 1975
 Ogilvie G. I., Lin D. N. C., 2007, *ApJ*, 661, 1180
 Orosz J. A., McClintock J. E., Aufdenberg J. P., Remillard R. A., Reid M. J., Narayan R., Gou L., 2011, *ApJ*, 742, 84
 Parker E. N., 1958, *ApJ*, 128, 677
 Parkinson P. M. S. et al., 2003, *ApJ*, 595, 333
 Penev K., Sasselov D., Robinson F., Demarque P., 2007, *ApJ*, 655, 1166
 Pols O. R., Schröder K.-P., Hurley J. R., Tout C. A., Eggleton P. P., 1998, *MNRAS*, 298, 525
 Portegies Zwart S. F., Verbunt F., 1996, *A&A*, 309, 179
 Portegies Zwart S. et al., 2009, *New Astron.*, 14, 369
 Pylyser E., Savonije G. J., 1988, *A&A*, 191, 57
 Rasio F. A., Tout C. A., Lubow S. H., Livio M., 1996, *ApJ*, 470, 1187
 Skumanich A., 1972, *ApJ*, 171, 565
 Tout C. A., Pols O. R., Eggleton P. P., Han Z., 1996, *MNRAS*, 281, 257
 Val Baker A. K. F., Norton A. J., Quaintrell H., 2005, *A&A*, 441, 685
 Valsecchi F., Rasio F. A., 2014, *ApJ*, 786, 102

- van der Meer A., Kaper L., van Kerkwijk M. H., van den Heuvel E. P. J., 2005, in Burderi L., Antonelli L. A., D'Antona F., di Salvo T., Israel G. L., Piersanti L., Tornambè A., Straniero O., eds, AIP Conf. Ser. Vol. 797, *Interacting Binaries: Accretion, Evolution, and Outcomes*. Am. Inst. Phys., New York, p. 623
- van Kerkwijk M. H., van Paradijs J., Zuiderwijk E. J., 1995, *A&A*, 303, 497
- Verbunt F., Phinney E. S., 1995, *A&A*, 296, 709
- Verbunt F., Zwaan C., 1981, *A&A*, 100, L7
- Weber E. J., Davis L., Jr, 1967, *ApJ*, 148, 217
- Wong T.-W., Valsecchi F., Fragos T., Kalogera V., 2012, *ApJ*, 747, 111
- Yungelson L. R., Lasota J.-P., Nelemans G., Dubus G., van den Heuvel E. P. J., Dewi J., Portegies Zwart S., 2006, *A&A*, 454, 559
- Zahn J. P., 1966, *Ann. Astrophys.*, 29, 489
- Zahn J.-P., 1975, *A&A*, 41, 329
- Zahn J.-P., 1977, *A&A*, 57, 383
- Zahn J.-P., 1989, *A&A*, 220, 112
- Zahn J.-P., 2008, in Goupil M.-J., Zahn J.-P., eds, *EAS Publications Series Vol. 29, Tidal Dissipation in Binary Systems*. ESA, Noordwijk, p. 67

This paper has been typeset from a $\text{\TeX}/\text{\LaTeX}$ file prepared by the author.